



# Next-generation GRAB sensors for monitoring dopaminergic activity in vivo

Fangmiao Sun<sup>1,2,7</sup>, Jingheng Zhou<sup>3,7</sup>, Bing Dai<sup>4,7</sup>, Tongrui Qian<sup>1,2</sup>, Jianzhi Zeng<sup>1,2,5</sup>, Xuelin Li<sup>1,2</sup>, Yizhou Zhuo<sup>1,2,5</sup>, Yajun Zhang<sup>1,2,5</sup>, Yipan Wang<sup>1,2</sup>, Cheng Qian<sup>1,2,6</sup>, Ke Tan<sup>1,2</sup>, Jiesi Feng<sup>1,2,5</sup>, Hui Dong<sup>1,2</sup>, Dayu Lin<sup>4</sup>✉, Guohong Cui<sup>3</sup>✉ and Yulong Li<sup>1,2,5</sup>✉

**Dopamine (DA) plays a critical role in the brain, and the ability to directly measure dopaminergic activity is essential for understanding its physiological functions. We therefore developed red fluorescent G-protein-coupled receptor-activation-based DA (GRAB<sub>DA</sub>) sensors and optimized versions of green fluorescent GRAB<sub>DA</sub> sensors. In response to extracellular DA, both the red and green GRAB<sub>DA</sub> sensors exhibit a large increase in fluorescence, with subcellular resolution, subsecond kinetics and nanomolar-to-submicromolar affinity. Moreover, the GRAB<sub>DA</sub> sensors resolve evoked DA release in mouse brain slices, detect evoked compartmental DA release from a single neuron in live flies and report optogenetically elicited nigrostriatal DA release as well as mesoaccumbens dopaminergic activity during sexual behavior in freely behaving mice. Coexpressing red GRAB<sub>DA</sub> with either green GRAB<sub>DA</sub> or the calcium indicator GCaMP6s allows tracking of dopaminergic signaling and neuronal activity in distinct circuits in vivo.**

DA is an essential monoamine neuromodulator produced primarily in the midbrain and released throughout the central nervous system. A multitude of brain functions are regulated by DA, including motor control, motivation, learning and memory, and emotional control<sup>1,2</sup>. Consistent with these key physiological roles, altered DA signaling has been implicated in a variety of brain disorders, including Parkinson's disease, addiction, schizophrenia, attention deficit hyperactivity disorder and post-traumatic stress disorder<sup>3</sup>. Thus, tools that can sense changes in DA concentration with high spatiotemporal resolution, high specificity and high sensitivity will facilitate studying the diverse functions that the dopaminergic system plays under both physiological and pathological conditions.

Techniques and tools for measuring DA dynamics such as microdialysis, electrochemical probes, reporter cells, gene expression-based assays and synthetic carbon nano-material-based probes show limitations in spatiotemporal resolution and/or molecular specificity<sup>4–10</sup>. Recently, we and others independently developed two series of genetically encoded, G-protein-coupled receptor-based DA sensors called GRAB<sub>DA</sub> and dLight, respectively<sup>11,12</sup>. Taking advantage of naturally occurring DA receptors, these sensors convert a ligand-stabilized conformational change in the DA receptor into an optical response via a conformation-sensitive fluorescent protein inserted in the receptor's third intracellular loop. Our first-generation DA receptor-based sensors called GRAB<sub>DA1m</sub> and GRAB<sub>DA1h</sub> were used to detect cell-type-specific DA dynamics in several organisms, including *Drosophila*, zebrafish, mice and zebra finches<sup>11,13–15</sup>. Here, we employed semi-rational engineering to modify the green fluorescent protein (GFP). The resulting second-generation sensors called GRAB<sub>DA2m</sub> and GRAB<sub>DA2h</sub> (abbreviated DA2m and DA2h, respectively) have a 2–3-fold higher

dynamic range and improved in vivo performance in comparison with the corresponding first-generation sensors.

Red fluorescent sensors have distinct and well-separated spectra from those of GFP-based sensors and blue-light-excitable channelrhodopsin 2 (ChR2), thus enabling the orthogonal readout of distinct neurochemical events, or simultaneous monitoring of neurotransmitter release and blue-light-mediated control of neuronal activity. Moreover, red fluorescent sensors require excitation with a relatively longer wavelength, providing additional advantages over GFP, including reduced phototoxicity, reduced background and deeper tissue penetration<sup>16,17</sup>. Starting with the DA D<sub>2</sub> receptor (D<sub>2</sub>R) and the conformation-sensitive red fluorescent protein cpmApple<sup>18</sup>, we generated red fluorescent DA sensors called rGRAB<sub>DA1m</sub> and rGRAB<sub>DA1h</sub> (abbreviated rDA1m and rDA1h, respectively), with a dynamic range similar to the corresponding first-generation green DA sensors.

## Results

**Development and in vitro characterization of DA sensors.** To develop red fluorescent DA sensors, we inserted cpmApple into the third intracellular loop of D<sub>2</sub>R and systematically optimized the insertion site, the linker sequences and the cpmApple module<sup>18–21</sup> (Extended Data Figs. 1 and 2), using both brightness and DA-induced change in fluorescence ( $\Delta F/F_0$ ) as our selection criteria. Screening over 2,000 sensor variants revealed the sensor with the highest fluorescence response; we called this sensor rDA0.5. Next, we used a rational strategy to introduce an iterative series of mutations in the D<sub>2</sub>R module of rDA0.5, generating versions with different apparent affinities to DA. The chosen sites for mutagenesis were implicated in affinity tuning<sup>22,23</sup> or located on the linkers or putative interface between the receptor backbone and cpmApple, which may be essen-

<sup>1</sup>State Key Laboratory of Membrane Biology, Peking University School of Life Sciences, Beijing, China. <sup>2</sup>PKU-IDG/McGovern Institute for Brain Research, Beijing, China. <sup>3</sup>Neurobiology Laboratory, National Institute of Environmental Health Sciences, National Institutes of Health, Research Triangle Park, NC, USA. <sup>4</sup>Neuroscience Institute, Department of Psychiatry, New York University School of Medicine, New York, NY, USA. <sup>5</sup>Peking-Tsinghua Center for Life Sciences, Beijing, China. <sup>6</sup>School of Life Sciences, Tsinghua University, Beijing, China. <sup>7</sup>These authors contributed equally: Fangmiao Sun, Jingheng Zhou, Bing Dai. ✉e-mail: [Dayu.Lin@nyulangone.org](mailto:Dayu.Lin@nyulangone.org); [cui@mail.nih.gov](mailto:cui@mail.nih.gov); [yulongli@pku.edu.cn](mailto:yulongli@pku.edu.cn)

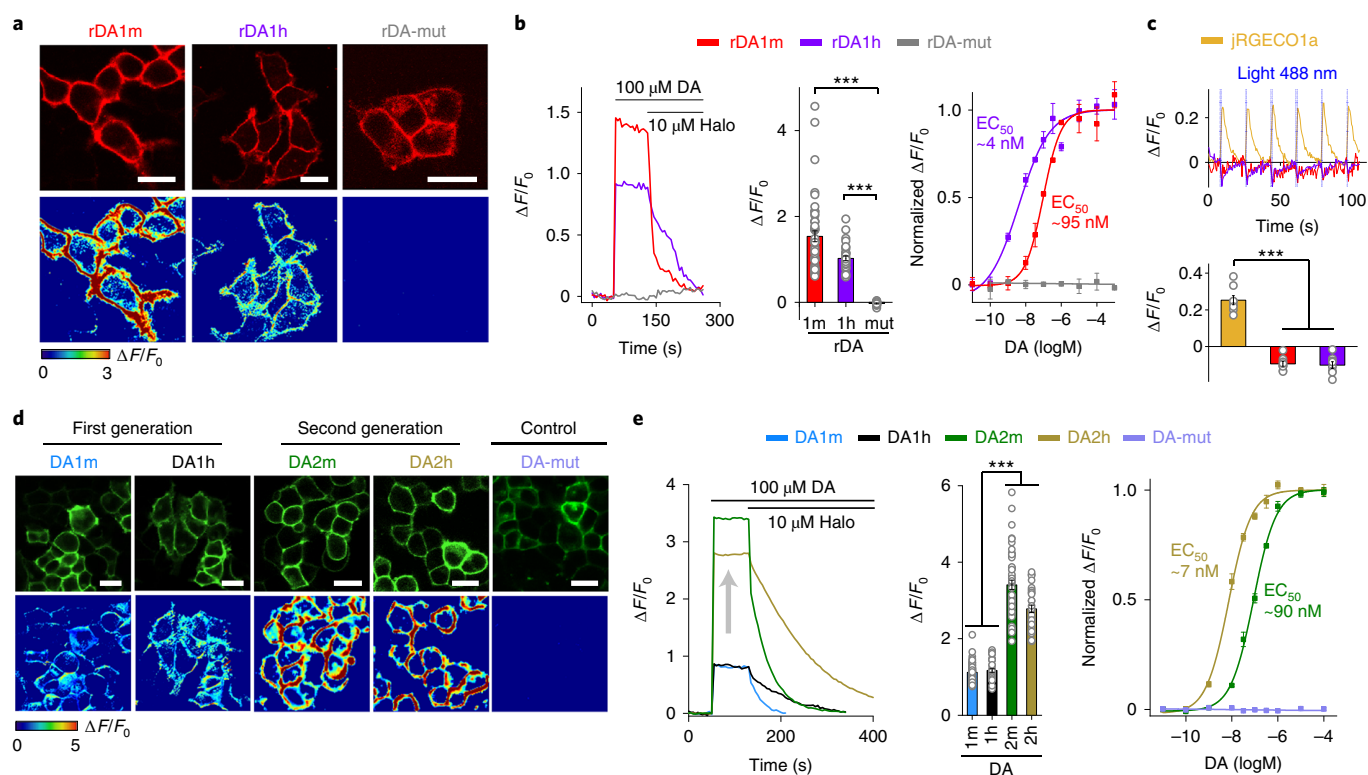


**Fig. 1 | Development of red fluorescent DA sensors and second-generation green fluorescent DA sensors. a**, Representative images of sensor expression (top) and response to 100  $\mu\text{M}$  DA (bottom) in HEK293T cells expressing the indicated sensor variants. Similar results were observed for more than ten cells. Scale bars, 20  $\mu\text{m}$ . **b**, Representative traces (left), group summary of peak  $\Delta F/F_0$  in response to 100  $\mu\text{M}$  DA (center) and normalized dose-response curves (right) in response to DA. Center,  $n = 46, 32, 17$  cells for rDA1m, rDA1h, rDA-mut. Right,  $n = 3$  wells with 200–400 cells per well. Two-tailed Student's  $t$ -test was performed.  $P = 3.52 \times 10^{-10}$  between rDA1m and rDA-mut;  $P = 4.79 \times 10^{-18}$  between rDA1h and rDA-mut. **c**, Representative traces (top) and group summary of  $\Delta F/F_0$  in response to blue light in cells expressing jRGECO1a, rDA1m or rDA1h. Bottom,  $n = 8, 9, 8$  cells for jRGECO1a, rDA1m, rDA1h. Two-tailed Student's  $t$ -test was performed.  $P = 1.23 \times 10^{-9}$  between jRGECO1a and rDA1m;  $P = 1.56 \times 10^{-8}$  between jRGECO1a and rDA1h. **d**, Representative images of sensor expression (top) and response to 100  $\mu\text{M}$  DA (bottom) in HEK293T cells expressing the indicated sensor variants. Similar results were observed for more than 20 cells. Scale bars, 20  $\mu\text{m}$ . **e**, Representative traces (left), group summary of peak  $\Delta F/F_0$  in response to 100  $\mu\text{M}$  DA (center) and normalized dose-response curves in response to DA (right). Center,  $n = 66, 36, 52, 33$  cells for DA1m, DA1h, DA2m, DA2h. Right,  $n = 3$  wells with 200–500 cells per well. Two-tailed Student's  $t$ -test was performed.  $P = 2.15 \times 10^{-41}$  between DA1m and DA2m;  $P = 8.34 \times 10^{-39}$  between DA1m and DA2h;  $P = 9.90 \times 10^{-26}$  between DA1h and DA2m;  $P = 4.66 \times 10^{-24}$  between DA1h and DA2h. Data are presented as the mean  $\pm$  s.e.m. in **b** (center and right), **c** (bottom) and **e** (center and right). \*\*\* $P < 0.001$ . 1h, the first-generation high-affinity sensor; 2h, the second-generation high-affinity sensor; 1m, the first-generation medium-affinity sensor; 2m, the second-generation medium-affinity sensor; mut, the DA-insensitive version.

tial for the structural coupling<sup>18</sup>. We generated the medium-affinity sensor rDA1m by introducing the K472<sup>6,29</sup>L mutation in rDA0.5, and the high-affinity sensor rDA1h by introducing the T205<sup>5,34</sup>M mutation in rDA1m. Finally, we generated a DA-insensitive version (rDA-mut) by introducing the C118<sup>3,36</sup>A and S193<sup>5,42</sup>N mutations in rDA1h (Extended Data Figs. 1a,b, 2a and 3 and Fig. 1). All three versions localized well on the cell membrane when expressed in HEK293T cells (Fig. 1a). rDA1m and rDA1h had a half-maximal effective concentration ( $EC_{50}$ ) of 95 nM and 4 nM, respectively (Fig. 1b). Moreover, the application of 100  $\mu\text{M}$  DA elicited a  $\sim 150\%$  and  $\sim 100\%$  increase in fluorescence of rDA1m and rDA1h, respectively, which was blocked by the  $D_2R$  antagonist haloperidol (Halo) (Fig. 1a,b). As expected, DA had no effect in cells expressing rDA-mut, even at the highest concentration tested (Fig. 1a,b).

Next, we asked whether the red DA sensors undergo photoactivation when expressed in HEK293T cells. Previous studies showed that cpmApple-based sensors can undergo photoactivation when illuminated with blue light<sup>24,25</sup>, preventing the combined use of these sensors with Chr2. We found that although the cpmApple-based red fluorescent calcium indicator jRGECO1a (ref. 25) had a  $\sim 25\%$  increase in fluorescence upon blue-light illumination (Fig. 1c), blue

light elicited a small decrease ( $\sim 10\%$ ) in the fluorescence of rDA1m and rDA1h, which is opposite to the on response and consequently less likely to interfere with DA detection. Moreover, we found that photostability of the red DA sensors was similar to or better than the photostability of several commonly used red fluorescent proteins when expressed in HEK293T cells (Extended Data Fig. 3j).

In parallel, we optimized our first-generation green fluorescent DA sensors by performing random mutagenesis at 32 sites in the cpEGFP module (Extended Data Figs. 1c and 2b). We chose these sites for the potential capability of improving the folding ability, brightness or structural coupling<sup>26–29</sup>. Screening  $\sim 1,000$  variants yielded DA2h, a high-affinity green fluorescent DA sensor. We then used this sensor to generate the medium-affinity DA2m and DA-insensitive DA-mut versions (Extended Data Figs. 1d, 2b and 3g). Compared with their corresponding first-generation DA1m and DA1h sensors, the second-generation green fluorescent DA sensors expressed in HEK293T cells had a 2–3-fold higher fluorescence increase ( $\Delta F/F_0 \sim 340\%$  for DA2m and  $\sim 280\%$  for DA2h) to 100  $\mu\text{M}$  DA while maintaining their apparent affinity to DA, with  $EC_{50}$  values of 90 nM and 7 nM for DA2m and DA2h, respectively (Fig. 1d,e). Finally, the DA-insensitive DA-mut sensor localized well

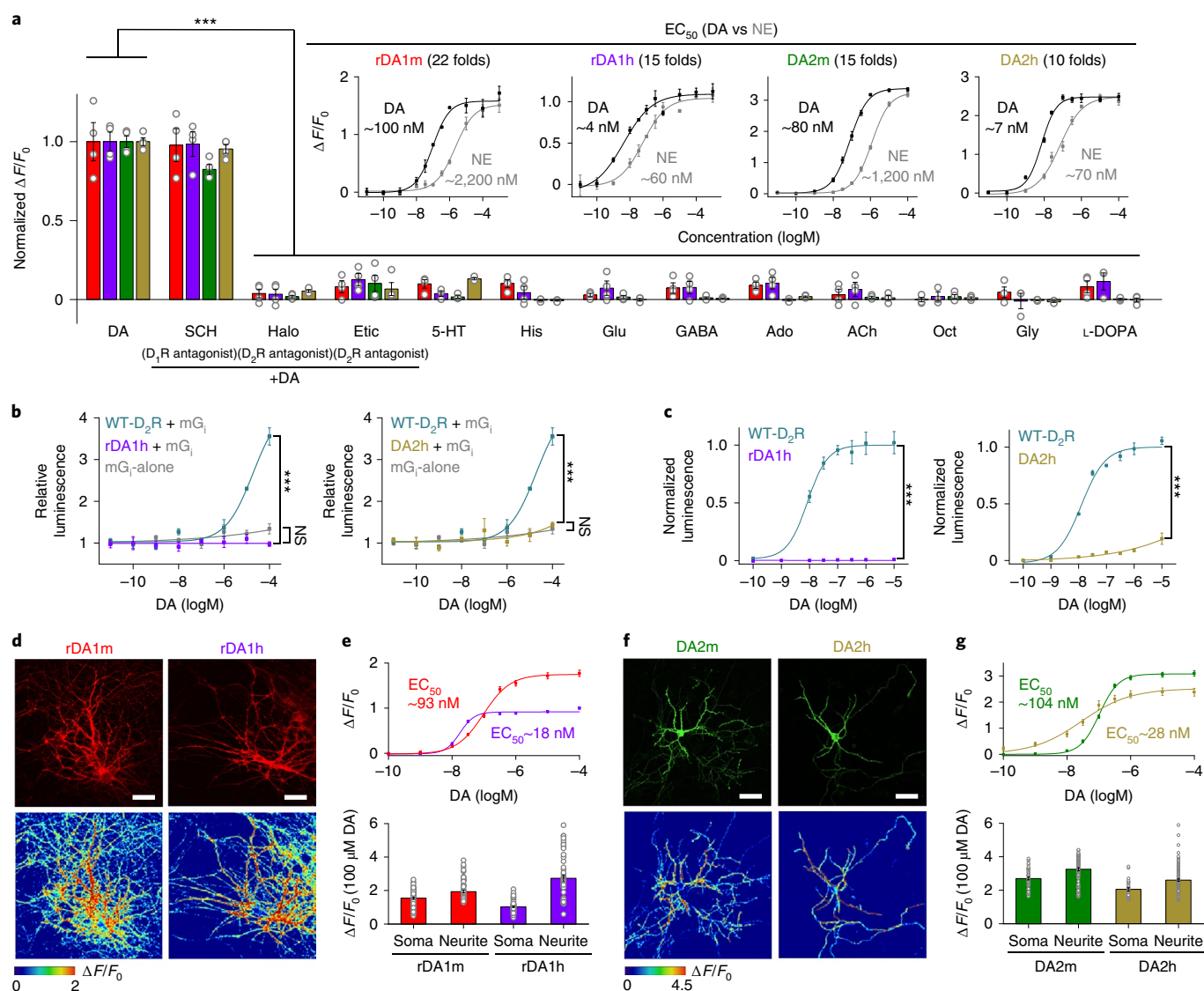


**Fig. 2 | Characterization of GRAB<sub>DA</sub> sensors in HEK293T cells and cultured rat cortical neurons. a**, Normalized  $\Delta F/F_0$  in sensor-expressing HEK293T cells following the application of DA alone, DA + SCH-23390 (SCH), DA + Halo, DA + eticlopride (Etic), serotonin (5-HT), histamine (His), glutamate (Glu), gamma-aminobutyric acid (GABA), adenosine (Ado), acetylcholine (ACh), octopamine (Oct), glycine (Gly) or L-DOPA (all applied at 1  $\mu$ M).  $n = 3$  wells for rDA1h in response to 5-HT, Oct, Gly and L-DOPA.  $n = 4$  wells for the others. Each well contains 200–1200 cells. The insets show dose–response curves for DA and norepinephrine (NE);  $n = 3$  wells with 200–800 cells per well each. Two-tailed Student’s  $t$ -test was performed. rDA1m,  $P = 0.8816, 0.0001, 0.0002, 0.0002, 0.0002, 8.94 \times 10^{-5}, 0.0001, 0.0001, 0.0001, 7.65 \times 10^{-5}, 0.0001$  and  $0.0002$  between DA and DA + SCH, DA + Halo, DA + Etic, 5-HT, His, Glu, GABA, Ado, ACh, Oct, Gly and L-DOPA, respectively. rDA1h,  $P = 0.8648, 4.12 \times 10^{-6}, 7.94 \times 10^{-6}, 2.34 \times 10^{-5}, 5.13 \times 10^{-6}, 7.89 \times 10^{-6}, 5.77 \times 10^{-6}, 6.37 \times 10^{-6}, 7.45 \times 10^{-6}, 2.63 \times 10^{-5}, 3.86 \times 10^{-5}$  and  $8.60 \times 10^{-5}$  between DA and DA + SCH, DA + Halo, DA + Etic, 5-HT, His, Glu, GABA, Ado, ACh, Oct, Gly and L-DOPA, respectively. DA2m,  $P = 0.0105, 1.99 \times 10^{-7}, 7.18 \times 10^{-6}, 1.92 \times 10^{-7}, 1.54 \times 10^{-7}, 2.00 \times 10^{-7}, 1.77 \times 10^{-7}, 1.55 \times 10^{-7}, 1.80 \times 10^{-7}, 2.46 \times 10^{-7}, 1.50 \times 10^{-7}$  and  $1.62 \times 10^{-7}$  between DA and DA + SCH, DA + Halo, DA + Etic, 5-HT, His, Glu, GABA, Ado, ACh, Oct, Gly and L-DOPA, respectively. DA2h,  $P = 0.2613, 2.90 \times 10^{-8}, 1.15 \times 10^{-6}, 4.20 \times 10^{-8}, 1.50 \times 10^{-8}, 1.83 \times 10^{-8}, 1.61 \times 10^{-8}, 1.80 \times 10^{-8}, 3.51 \times 10^{-8}, 1.87 \times 10^{-8}, 1.46 \times 10^{-8}$  and  $2.83 \times 10^{-8}$  between DA and DA + SCH, DA + Halo, DA + Etic, 5-HT, His, Glu, GABA, Ado, ACh, Oct, Gly and L-DOPA, respectively. **b**, Luciferase complementation assay for assessing  $G_i$  coupling.  $n = 3$  wells each. The luminescence signals are normalized against the luminescence signals measured in the control buffer-treated cells. Cells expressing  $mG_i$  alone serve as the control. Two-tailed Student’s  $t$ -test was performed.  $P = 9.87 \times 10^{-5}$  between rDA1h and WT-D<sub>2</sub>R;  $P = 0.1124$  between rDA1h and  $mG_i$ -alone;  $P = 0.0001$  between DA2h and WT-D<sub>2</sub>R;  $P = 0.2836$  between DA2h and  $mG_i$ -alone. **c**, TANGO assay for measuring  $\beta$ -arrestin coupling.  $n = 3$  wells each. The maximum luminescence signals of WT-D<sub>2</sub>R are normalized to 1. Two-tailed Student’s  $t$ -test was performed.  $P = 0.0004$  between rDA1h and WT-D<sub>2</sub>R;  $P = 0.0001$  between DA2h and WT-D<sub>2</sub>R. **d**, Representative images of sensor expression (top) and response to 100  $\mu$ M DA (bottom) in neurons expressing the indicated sensors. Similar results were observed for more than 30 neurons. Scale bars, 10  $\mu$ m. **e**, Dose–response curves (top) and group summary (bottom) of the responses measured in the soma and neurites of sensor-expressing neurons. Top,  $n = 34$  and 14 neurons for rDA1m and rDA1h. Bottom,  $n = 59$  and 68 ROIs from 59 neurons for rDA1m (soma) and rDA1m (neurite);  $n = 58$  and 58 ROIs from 58 neurons for rDA1h (soma) and rDA1h (neurite). **f**, Representative images of sensor expression (top) and response to 100  $\mu$ M DA (bottom) in neurons expressing the indicated sensors. Similar results were observed for more than 20 neurons. Scale bars, 10  $\mu$ m. **g**, Dose–response curves (top) and group summary (bottom) of the responses measured in the soma and neurites of sensor-expressing neurons. Top,  $n = 32$  and 21 neurons for DA2m and DA2h. Bottom,  $n = 54$  and 85 ROIs from 54 neurons for DA2m (soma) and DA2m (neurite);  $n = 30$  and 145 ROIs from 30 neurons for DA2h (soma) and DA2h (neurite). Data are presented as the mean  $\pm$  s.e.m. in **a, b, c, e** and **g**. \*\*\* $P < 0.001$ ; NS, not significant; ROI, region of interest; WT-D<sub>2</sub>R, wild-type D<sub>2</sub> receptor.

on the cell membrane of HEK293T cells but did not respond to DA (Fig. 1d,e).

We further characterized the specificity, kinetics and downstream coupling of our DA sensors in HEK293T cells. With respect to specificity, the DA-induced signals of both the red and green DA sensors were blocked by the D<sub>2</sub>R-specific antagonists Halo and eticlopride, but not the D<sub>1</sub>R antagonist SCH-23390. The four DA sensors exhibited negligible responses to a variety of tested neurotransmitters and neuromodulators (serotonin, histamine, glutamate, GABA, adenosine, acetylcholine, octopamine, glycine, L-DOPA) (Fig. 2a and Extended Data Fig. 4). Although norepinephrine is structurally similar to DA, both the red and green DA sensors were 10–20-fold more selective for DA over norepinephrine (Fig. 2a and Extended Data Fig. 4), suggesting good selectivity for DA of our sensors at physiologically relevant concentrations.

We next characterized the kinetics of the DA sensors using rapid line-scanning in response to a local puff of DA (to measure the time constant of the on response ( $\tau_{\text{on}}$ )) followed by Halo (to measure the time constant of the off response ( $\tau_{\text{off}}$ )) to sensor-expressing HEK293T cells.  $\tau_{\text{on}}$  was <100 ms for all four DA sensors while the high-affinity versions had relatively slower off kinetics compared with their corresponding medium-affinity counterparts (Extended Data Fig. 3a–f).

To examine whether our DA sensors couple to signaling pathways downstream of the DA receptors the sensors are based on, we used the luciferase complementation assay<sup>30</sup> and TANGO assay<sup>31</sup> to measure activation of the G<sub>i</sub> and  $\beta$ -arrestin pathways, respectively (Fig. 2b,c). When expressed in HEK293T cells, both the rDA1h and DA2h sensors exhibited minimal downstream coupling in both assays (Fig. 2b,c). In contrast, wild-type D<sub>2</sub>R as a control showed robust coupling (Fig. 2b,c). Furthermore, GTP $\gamma$ S treatment did not alter the EC<sub>50</sub> to DA for rDA1h and DA2h sensors (Extended Data Fig. 5a,b). When imaging for 2 h or 1 h in sensor-expressing cultured rat cortical neurons or transgenic flies, respectively, we did not observe a substantial fluorescent decrease, indicating minimal desensitization in both cases (Extended Data Fig. 5c–m). Taken together, these results indicate that our DA sensors show minimal coupling to downstream signaling pathways.

In cultured neurons, both the red and green DA sensors readily localized to the cell membrane and responded well to DA (Fig. 2d–g).

Lastly, we compared the properties of the second-generation green fluorescent DA2m sensor with D<sub>1</sub>R-based dLight1.1, dLight1.2 and dLight1.3b sensors (Extended Data Fig. 6a–m). When expressed in cultured cells, DA2m had a higher apparent affinity to DA, higher basal and maximal brightness, and higher  $\Delta F/F_0$  than dLight series, except that dLight1.3b has a larger maximal  $\Delta F/F_0$ . However, DA2m has a higher  $\Delta F/F_0$  at <1  $\mu$ M DA concentration

and exhibits overall higher signal-to-noise ratio (SNR). On the other hand, the D<sub>1</sub>R-based dLight series have faster off kinetics<sup>12</sup>.

**Imaging of DA release in acute mouse brain slices.** Next, we examined whether our DA sensors can be used to measure the release of endogenous DA in acute brain slices (Fig. 3). We injected adeno-associated viruses (AAVs) for expressing rDA1m, rDA1h or DA2m into the nucleus accumbens (NAc), which receives strong innervation from midbrain dopaminergic neurons (DANs) (Fig. 3a,b). At 2 weeks after injection, we prepared acute brain slices and used two-photon imaging combined with electrical stimulation to measure stimulus-evoked DA release (Fig. 3a). Electrical stimuli delivered at 20 Hz induced fluorescence responses in the NAc, which scaled with the number of pulses delivered and which were blocked by Halo (Fig. 3c,e). We also measured the sensors' kinetics while applying ten pulses at 100 Hz. The  $\tau_{\text{on}}$  and  $\tau_{\text{off}}$  values for the three sensors were in the range of 0.08–0.15 s and 5.2–11.8 s, respectively (Fig. 3d).

To test whether the red fluorescent DA sensor is spectrally compatible with a green fluorescent calcium sensor, we coexpressed axon-targeted GCaMP6s (ref. <sup>32</sup>) in the ventral tegmental area and rDA1m in the NAc, then simultaneously imaged calcium and DA in the NAc during 20-Hz electrical stimulation (Fig. 3f,g). The electrical stimulation evoked robust fluorescence increases of both GCaMP6s and rDA1m and the magnitudes of increases were highly correlated (Fig. 3k). Application of the D<sub>2</sub>R antagonist Halo blocked the rDA1m response but had no effect on the GCaMP6s response (Fig. 3h–j). Taken together, these data indicate that the rDA1m, rDA1h and DA2m sensors can detect dopaminergic activity in brain slices. Moreover, our results confirm that the red fluorescent DA sensors are spectrally compatible with green fluorescent probes, allowing dual-color imaging.

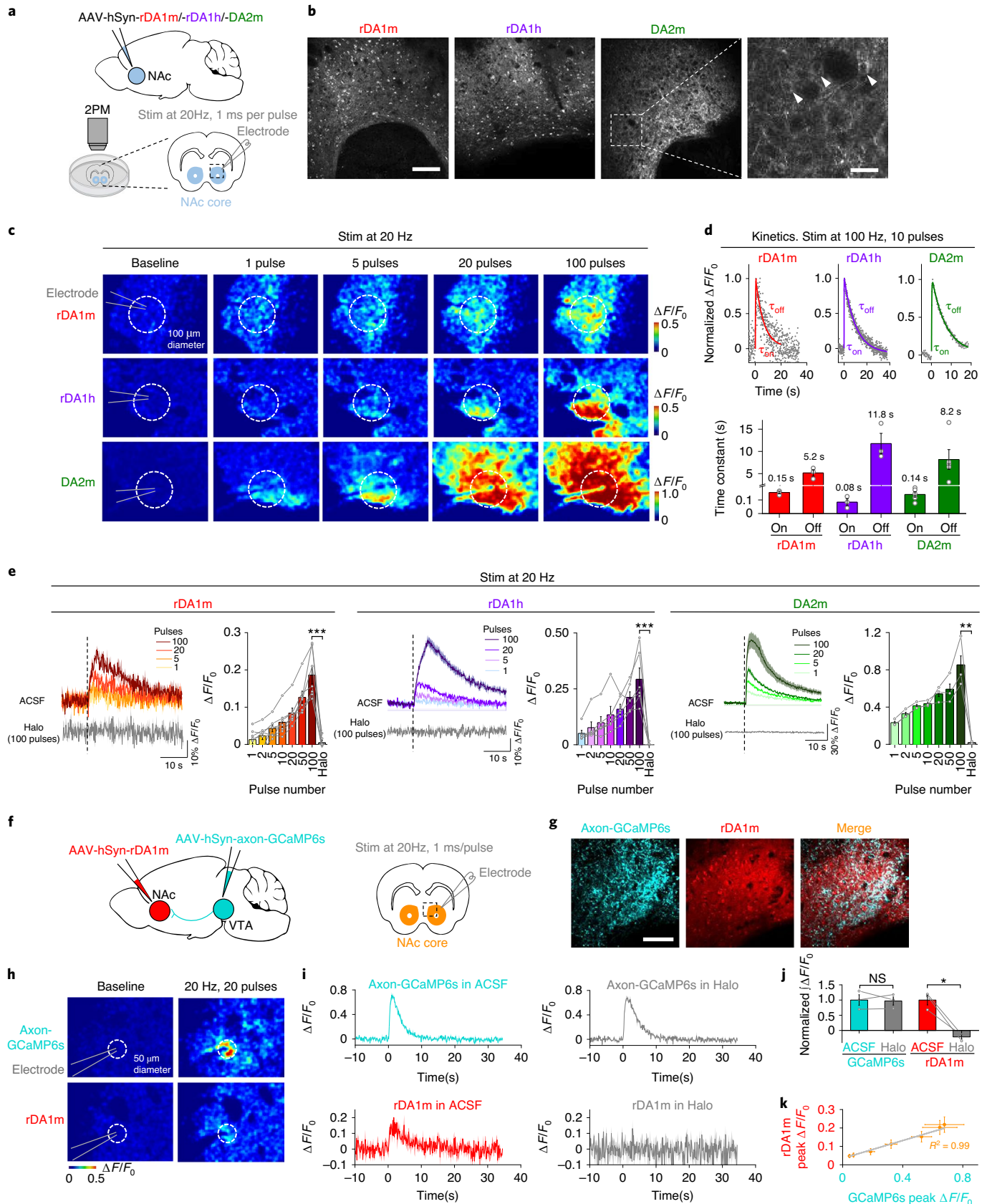
**In vivo imaging of DA in *Drosophila*.** In *Drosophila*, dopaminergic activity in the mushroom body (MB) is both necessary and sufficient for associative learning of an odor and an aversive experience, for example, body shock<sup>33–36</sup>. We generated transgenic *Drosophila* expressing rDA1m in Kenyon cells in the MB and measured the fluorescence level of the rDA1m sensor using in vivo two-photon imaging while presenting physiologically relevant stimuli (Fig. 4a,b). When we delivered either the odorant or body shock, we observed a time-locked fluorescence increase in the MB medial lobe; this increase was blocked by pretreating the animals with Halo (Fig. 4c,d) and was not observed in flies expressing the DA-insensitive rDA-mut sensor. The endogenous signal did not saturate the rDA1m sensor's response, as application of 100  $\mu$ M DA caused a substantially larger, sustained increase in fluorescence (Fig. 4e).

**Fig. 3 | GRAB<sub>DA</sub> sensors can be used to measure DA release in acute mouse brain slices.** **a**, Schematic illustration depicting the experimental design for panels **b–e**. **b**, Representative fluorescence images showing the expression of sensors in the NAc. The arrowheads indicate the somas of individual neurons. Similar results were observed for 3–4 mice. Scale bars, 100  $\mu$ m (left) and 20  $\mu$ m (right). **c**, Responses to electrical stimulation measured in sensor-expressing brain slices. The dashed circles indicate the ROIs used to analyze the signals. **d**, Representative traces showing the normalized  $\Delta F/F_0$  (top) and group summary of  $\tau_{\text{on}}$  and  $\tau_{\text{off}}$  (bottom) in response to ten electrical stimuli applied at 100 Hz. The data were processed with 2 $\times$  binning. Each trace was fitted with a single-exponential function to determine  $\tau_{\text{on}}$  and  $\tau_{\text{off}}$ .  $n=3$  slices from two mice for rDA1m,  $n=3$  slices from two mice for rDA1h and  $n=5$  slices from three mice for DA2m. **e**, Representative traces and group summary of the  $\Delta F/F_0$  in response to electrical stimulation.  $n=7$  slices from four mice for rDA1m,  $n=6$  slices from four mice for rDA1h and  $n=3$  slices from two mice for DA2m. Two-tailed Student's  $t$ -test was performed.  $P=2.97 \times 10^{-5}$ , 0.0002 and 0.0061 for rDA1m, rDA1h and DA2m. **f**, Schematic illustration depicting the experimental design for panels **g–j**. **g**, Representative fluorescence images showing the expression of GCaMP6s and rDA1m in the NAc. Similar results were observed for three mice. Scale bar, 100  $\mu$ m. **h**, Response images of axon-GCaMP6s and rDA1m following electrical stimulation. The dashed circles indicate the ROIs used to analyze the signals. **i, j**, Representative traces (**i**) and group summary (**j**) of the  $\Delta F/F_0$  in response to electrical stimulation.  $n=3$  slices from three mice. Two-tailed Student's  $t$ -test was performed.  $P=0.8361$  and  $P=0.0244$  for GCaMP6s and rDA1m. **k**, The peak  $\Delta F/F_0$  of rDA1m plotted against the peak  $\Delta F/F_0$  of axon-GCaMP6s in response to various numbers of pulses applied at 20 Hz. The data were fitted to a linear function.  $n=8$  slices from three mice. Average traces shaded with  $\pm$ s.e.m. from one slice are shown for representation in **e** and **i**. Data are presented as the mean  $\pm$ s.e.m. in **d** (bottom), **e, j** and **k**.  $**P < 0.01$ ;  $***P < 0.001$ . ACSF, artificial cerebrospinal fluid; 2PM, two-photon microscopy.



We then compared the *in vivo* performance between the first-generation and second-generation green fluorescent DA sensors in flies. Electrical stimulation of the MB medial lobe elicited a robust fluorescence increase in nearby DA sensor-expressing DANs, with a

higher response observed in DA2m-expressing flies compared with DA1m-expressing flies (Fig. 4f,g). The temporal dynamics of the DA2m and DA1m responses ( $\tau_{on}$  and  $\tau_{off}$ ) were similar to each other and both responses were blocked by Halo (Fig. 4h–l). The spatial pat-



terns of the responses in the MB during odorant or body shock delivery were also similar between DA2m- and DA1m-expressing flies<sup>11</sup>, with higher responses consistently observed in DA2m-expressing flies (Fig. 4m–o and Supplementary Video 1). In a separate experiment, we compared the *in vivo* performance of DA2m with dLight1.3b, which has the highest dynamic range among the dLight series of sensors, and found that DA2m produced a threefold-larger response than dLight1.3b (Extended Data Fig. 6n–r).

Previous studies have found that the *Drosophila* MB is innervated by 15 DAN subgroups, with each lobe containing axons from approximately one dozen to two dozen DANs<sup>37–39</sup>. We asked whether our DA2m sensor could detect DA release in individual MB compartments, even when the source of DA is a single neuron. We coexpressed the red-light-activated channelrhodopsin CsChrimson<sup>40</sup> in DANs and DA2m in Kenyon cells. We then optically activated the only DAN neuron innervating the  $\gamma 2\alpha 1$  compartment or the 8–21 neurons innervating the  $\gamma 5$  compartment while measuring DA2m fluorescence (Fig. 4p). The change in DA2m fluorescence was both time-locked to the CsChrimson activation and spatially confined to the respective compartments, suggesting functional independence among MB compartments (Fig. 4q,r).

To examine any potential coupling of the DA2m sensor and the  $G_i$  pathway *in vivo*, we measured cAMP levels, as a proxy for  $G_i$  signaling, using the red fluorescent cAMP sensor Pink-Flamindo<sup>41</sup>. We found that the presence of the DA2m sensor had no significant ( $P = 0.7332$ , two-tailed Student's *t*-test) effect on cAMP production during body shock (Extended Data Fig. 7a–f). We further assessed odor-evoked calcium signaling in Kenyon cells using GCaMP5 (ref. <sup>42</sup>), and found that the concurrently expressed rDA1m sensor had no significant effect on the  $Ca^{2+}$  response (Extended Data Fig. 7g–l;  $P = 0.607$  in Extended Data Fig. 7k;  $P = 0.601$ , 0.735 for  $\tau_{on}$ ,  $\tau_{off}$  in Extended Data Fig. 7l; two-tailed Student's *t*-test). Thus, the GRAB<sub>DA</sub> sensors have minimal effects on endogenous signaling pathways *in vivo*.

**Detection of DA release in freely behaving mice.** To test the performance of our sensors *in vivo* in mice, we measured DA dynamics

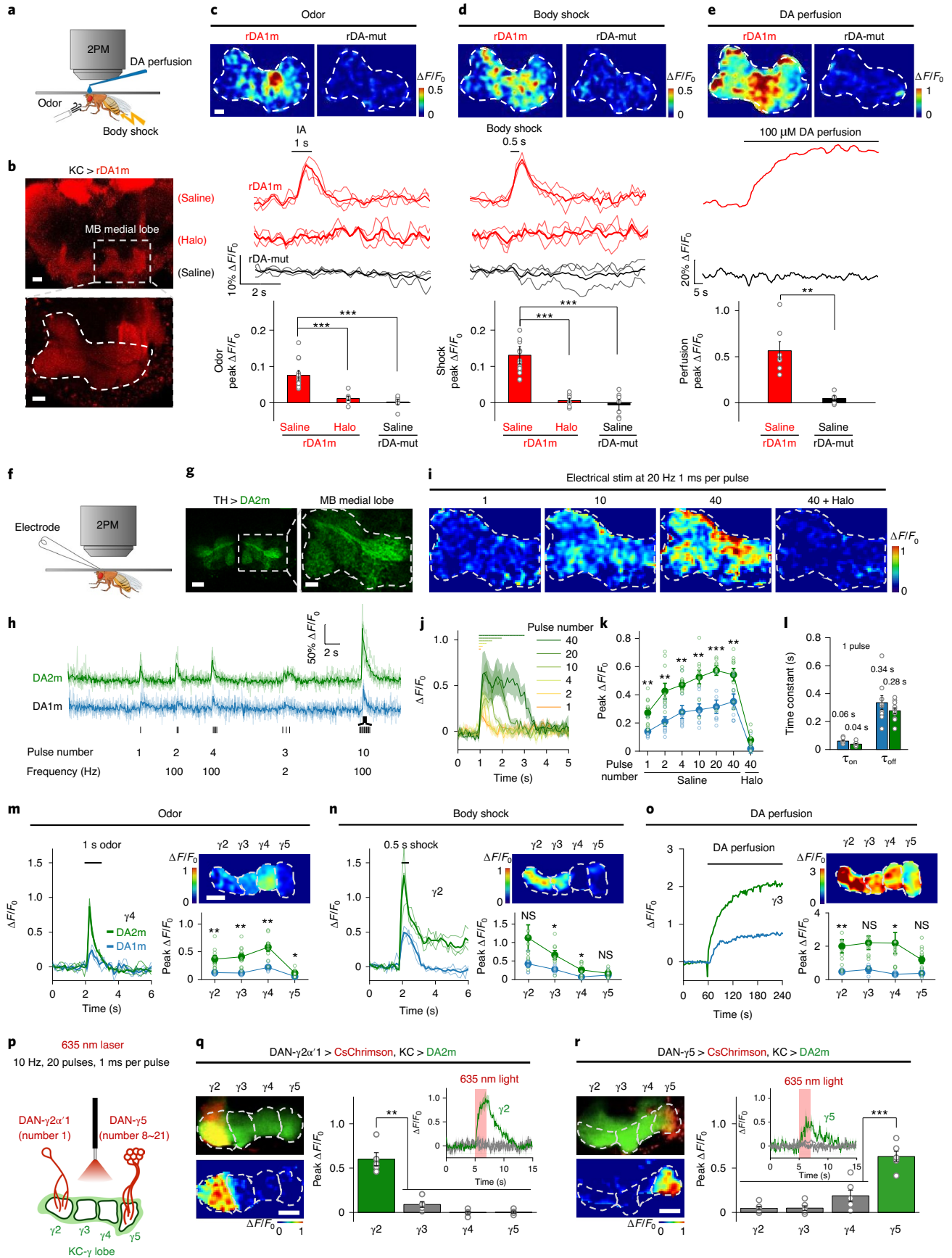
in the dorsal striatum, the main target of dopaminergic projections from the substantia nigra pars compacta (SNc), by expressing the optogenetic tool C1V1 (ref. <sup>43</sup>) in the SNc and various DA sensors in the dorsal striatum (Fig. 5). As an internal control for the red and green fluorescent sensors, we also coexpressed EGFP or tdTomato, respectively, in the dorsal striatum (Fig. 5a,b). C1V1-mediated optogenetic activation of DANs in the SNc elicited a robust transient increase in DA sensor fluorescence (Fig. 5d–g), but not in the DA-insensitive control rDA-mut fluorescence (Fig. 5c,h). The evoked response was prolonged by the DA transporter blocker methylphenidate and blocked by the  $D_2R$  antagonist eticlopride (Fig. 5d–g,i–l), but was unaffected by the norepinephrine transporter blocker desipramine and the  $\alpha_2$ -adrenergic receptor antagonist yohimbine (Extended Data Fig. 8). Thus, our DA sensors can detect optogenetically induced DA release in freely moving mice.

To show GRAB<sub>DA</sub> performance relative to downstream events, we expressed DA2m in the dorsal striatum of Drd1-Cre mice that also expressed the red calcium indicator jRGECO1a in direct-pathway striatal neurons (Extended Data Fig. 9). During simultaneous GRAB<sub>DA</sub> and jRGECO1a recordings in freely behaving mice, we observed inverted correlation of the temporal profiles between the DA signal and the direct-pathway neural activity.

To compare DA2h and DA1h sensor performance during natural behaviors, we expressed DA1h and DA2h in opposite sides of the NAc core, and performed bilateral fiber photometry recording during male mating<sup>11</sup> (Fig. 6a,b). We found that the DA1h and DA2h signals were closely correlated in time while the DA2h sensor had a substantially higher fluorescence change ( $\Delta F/F_0$ ) than DA1h during various stages of mating (Fig. 6c–f). This difference is not due to endogenous difference of DA release between the left and right NAc as simultaneous bilateral recording of DA signals using DA2h only reveals no laterality in the response patterns during male sexual behaviors (Extended Data Fig. 10a–c).

We next compared the performance of red fluorescent rDA1m sensor with that of the green fluorescent DA sensor, DA2h. We coinjected viruses expressing rDA1m and DA2h into the NAc core and performed dual-color fiber photometry recording (Fig. 6g,h).

**Fig. 4 | *In vivo* two-photon imaging of DA dynamics in *Drosophila* using GRAB<sub>DA</sub> sensors.** **a**, Schematic illustration depicting the experimental setup for imaging fluorescence changes in response to various stimuli. **b**, Representative fluorescence images of rDA1m expressed in Kenyon cells (KCs), with an expanded view of the olfactory MB medial lobe. Similar results were observed for 15 flies. Scale bars, 20  $\mu\text{m}$  (top) and 10  $\mu\text{m}$  (bottom). **c–e**, Representative images (top; the dashed area indicates the MB medial lobe), traces (center) and group summary (bottom) of  $\Delta F/F_0$  in response to odorant (**c**), body shock (**d**) and DA perfusion (**e**). Scale bar, 10  $\mu\text{m}$ . **c**,  $n = 15$ , 7 and 6 flies for rDA1m (saline), rDA1m (Halo) and rDA-mut. **d**,  $n = 15$ , 7 and 8 flies for rDA1m (saline), rDA1m (Halo) and rDA-mut (saline). **e**,  $n = 7$  and 5 flies for rDA1m (saline) and rDA-mut (saline). Two-tailed Student's *t*-test was performed. **c**,  $P = 0.0002$  between rDA1m (saline) and rDA1m (Halo);  $P = 6.70 \times 10^{-6}$  between rDA1m (saline) and rDA-mut (saline). **d**,  $P = 5.48 \times 10^{-5}$  between rDA1m (saline) and rDA1m (Halo);  $P = 1.71 \times 10^{-6}$  between rDA1m (saline) and rDA-mut (saline). **e**,  $P = 0.0016$  between rDA1m (saline) and rDA-mut (saline). **f**, Schematic illustration depicting the experimental setup for imaging electrical stimulation-evoked DA release. **g**, Representative fluorescence images of DA2m expressed in DANs, with an expanded view of the MB medial lobe. Similar results were observed for ten flies. Scale bars, 20  $\mu\text{m}$  (left) and 10  $\mu\text{m}$  (right). **h**, Representative traces of DA2m and DA1m fluorescence; where indicated, electrical stimuli were applied. **i, j**, Representative images (**i**) and traces (**j**) of DA2m  $\Delta F/F_0$  in response to electrical stimuli. Similar results were observed for ten flies. **k**, Group summary of DA2m and DA1m  $\Delta F/F_0$  in response to electrical stimuli.  $n = 9$ , 5, 10 and 10 flies for DA1m (saline), DA1m (Halo), DA2m (saline) and DA2m (Halo). Two-tailed Student's *t*-test was performed.  $P = 0.0023$ , 0.0047, 0.0025, 0.0014, 0.0002 and 0.0091 for 1, 2, 4, 10, 20 and 40 pulse(s), respectively. **l**, Kinetics ( $\tau_{on}$  and  $\tau_{off}$ ) of DA2m and DA1m in response to a single electrical stimulus.  $n = 9$  and 10 flies for DA1m and DA2m. **m–o**, Representative traces (left), fluorescence images (top right) and group summary (bottom right) of the indicated MB lobe compartments in response to odorant (**m**), body shock (**n**) and 1 mM DA perfusion (**o**). **m**,  $n = 4$  and 9 flies for DA1m and DA2m. **n**,  $n = 6$  and 8 flies for DA1m and DA2m. **o**,  $n = 3$  and 11 flies for DA1m and DA2m. Two-tailed Student's *t*-test was performed. **m**,  $P = 0.0070$ , 0.0024, 0.0091 and 0.0171 for  $\gamma 2$ ,  $\gamma 3$ ,  $\gamma 4$  and  $\gamma 5$ , respectively. **n**,  $P = 0.0910$ , 0.0137, 0.0207 and 0.3808 for  $\gamma 2$ ,  $\gamma 3$ ,  $\gamma 4$  and  $\gamma 5$ , respectively. **o**,  $P = 0.0033$ , 0.0701, 0.0150 and 0.0990 for  $\gamma 2$ ,  $\gamma 3$ ,  $\gamma 4$  and  $\gamma 5$ , respectively. **p**, Schematic illustration depicting the strategy for imaging optogenetically induced DA release. DA2m is expressed in the KCs, and CsChrimson is expressed in either the  $\gamma 2$  or  $\gamma 5$  MB compartment (with the number of innervating cells indicated). **q, r**, Representative fluorescence images (top left), response images (bottom left), representative traces (top right) and group summary (bottom right) of DA2m fluorescence in the  $\gamma 2$  (**q**) and  $\gamma 5$  (**r**) MB compartments in response to optogenetic stimulation. Scale bars, 20  $\mu\text{m}$ . **q**,  $n = 5$  flies. **r**,  $n = 6$  flies. Two-tailed Student's *t*-test was performed. **q**,  $P = 0.0035$ , 0.0012 and 0.0013 between  $\gamma 2$  and  $\gamma 3$ ,  $\gamma 4$  and  $\gamma 5$ , respectively. **r**,  $P = 0.0002$ , 0.0003 and 0.0001 between  $\gamma 5$  and  $\gamma 2$ ,  $\gamma 3$  and  $\gamma 4$ , respectively. The group data for DA1m shown in panels **k, m, n** and **o** were reproduced from Sun et al.<sup>11</sup> with permission. Average traces (bold) overlaid with single-trial traces (light) from one fly are shown for representation in **c, d, h, m** and **n**. Average traces shaded with  $\pm$ s.e.m. from one fly are shown for representation in **j, q** and **r**. Data are presented as the mean  $\pm$ s.e.m. in **c, d, e, k, l, m, n, o, q** and **r**. \* $P < 0.05$ ; \*\* $P < 0.01$ ; \*\*\* $P < 0.001$ .



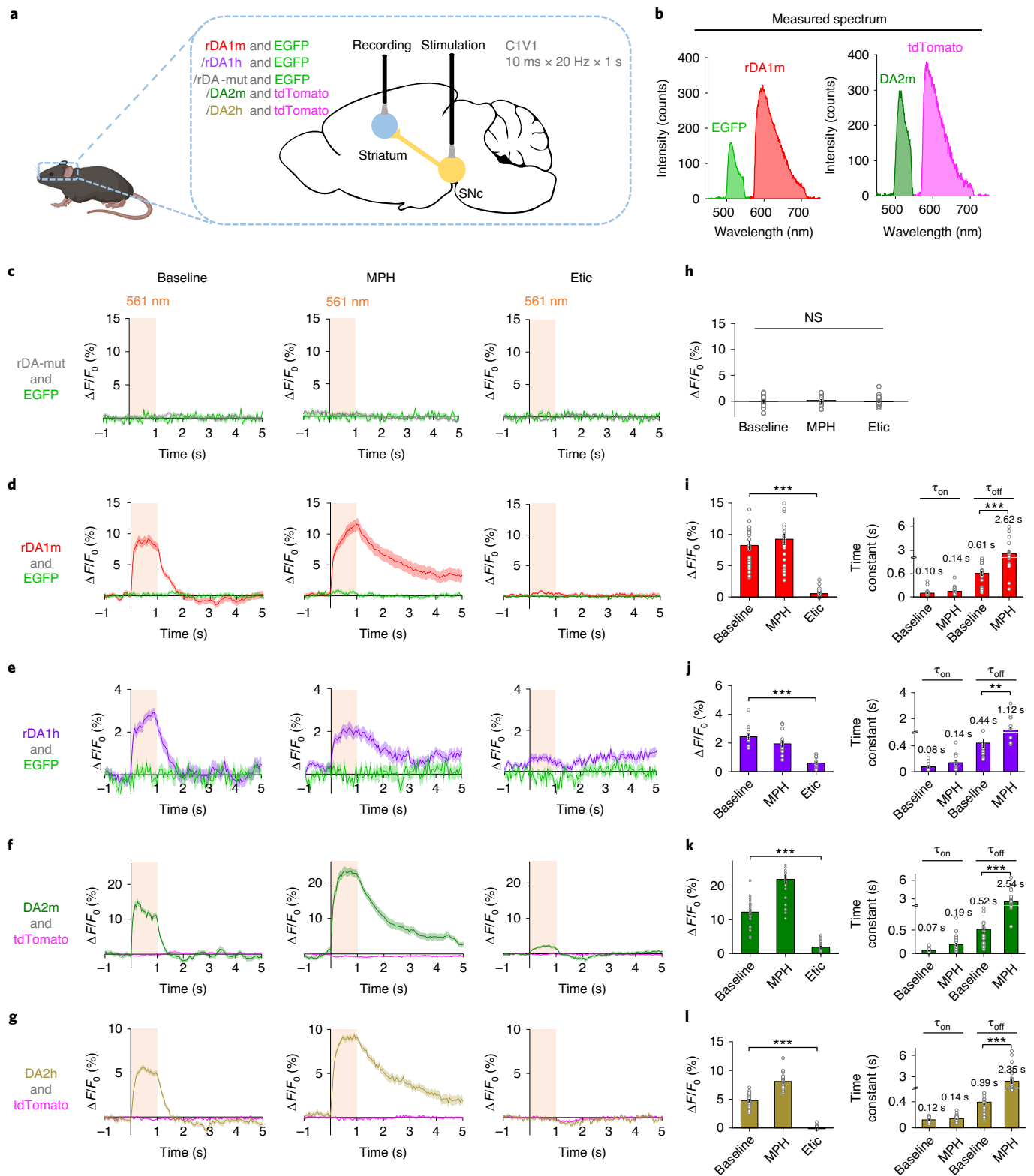


**Fig. 5 | GRAB<sub>DA</sub> sensors can detect optogenetically induced nigrostriatal DA release in freely moving mice. a**, Schematic illustration depicting the experimental setup. **b**, Measured emission spectra in vivo using fiber photometry. **c–g**, Average  $\Delta F/F_0$  traces of the indicated sensors and fluorescent proteins during optogenetic stimulation under control conditions (left) or in the presence of methylphenidate (MPH) or eticlopride (Etic). **h–l**, Group summary of  $\Delta F/F_0$  and time constants (where applicable) for the corresponding sensors in panels **c–g**, respectively.  $n = 30$  trials from six hemispheres of three mice for rDA-mut.  $n = 30$  trials from six hemispheres of six mice for rDA1m.  $n = 15$  trials from three hemispheres of three mice for rDA1h.  $n = 30$  trials from six hemispheres of three mice for DA2m.  $n = 25$  trials from five hemispheres of four mice for DA2h. Two-tailed Student's *t*-test was performed. **h**,  $P = 0.6066$  between baseline and MPH;  $P = 0.7130$  between baseline and Etic;  $P = 0.3216$  between MPH and Etic. **i**, Left,  $P = 1.27 \times 10^{-16}$ ; right,  $P = 2.98 \times 10^{-15}$ . **j**, Left,  $P = 7.07 \times 10^{-10}$ ; right,  $P = 0.0034$ . **k**, Left,  $P = 7.86 \times 10^{-21}$ ; right,  $P = 1.07 \times 10^{-6}$ . **l**, Left,  $P = 1.86 \times 10^{-25}$ ; right,  $P = 2.06 \times 10^{-7}$ . Average traces shaded with  $\pm$ s.e.m. are shown in **c–g**. Data are presented as the mean  $\pm$ s.e.m. in **h–l**. \*\* $P < 0.01$ ; \*\*\* $P < 0.001$ .



While the dynamic range ( $\Delta F/F_0$ ) of rDA1m is smaller than that of DA2h (Fig. 6i–l), rDA1m and DA2h detected qualitatively similar DA release during sexual behavior based on Z-scored signals (Extended Data Fig. 10d–f). The moment-to-moment correlation coefficient between rDA1m and DA2h is similar to that between DA1h and DA2h (Fig. 6d,j). Importantly, we did not observe cross-talk between the red and green DA sensors as we did not detect a signal in the red channel when we delivered only 470-nm light

and vice versa (Extended Data Fig. 10g–j). Taken together, rDA1m is capable of detecting DA release in vivo during natural behaviors and the behavior-related DA responses detected by the red and green DA sensors are qualitatively similar.

## Discussion

Here, we report the development and characterization of a set of genetically encoded DA sensors. The availability of both

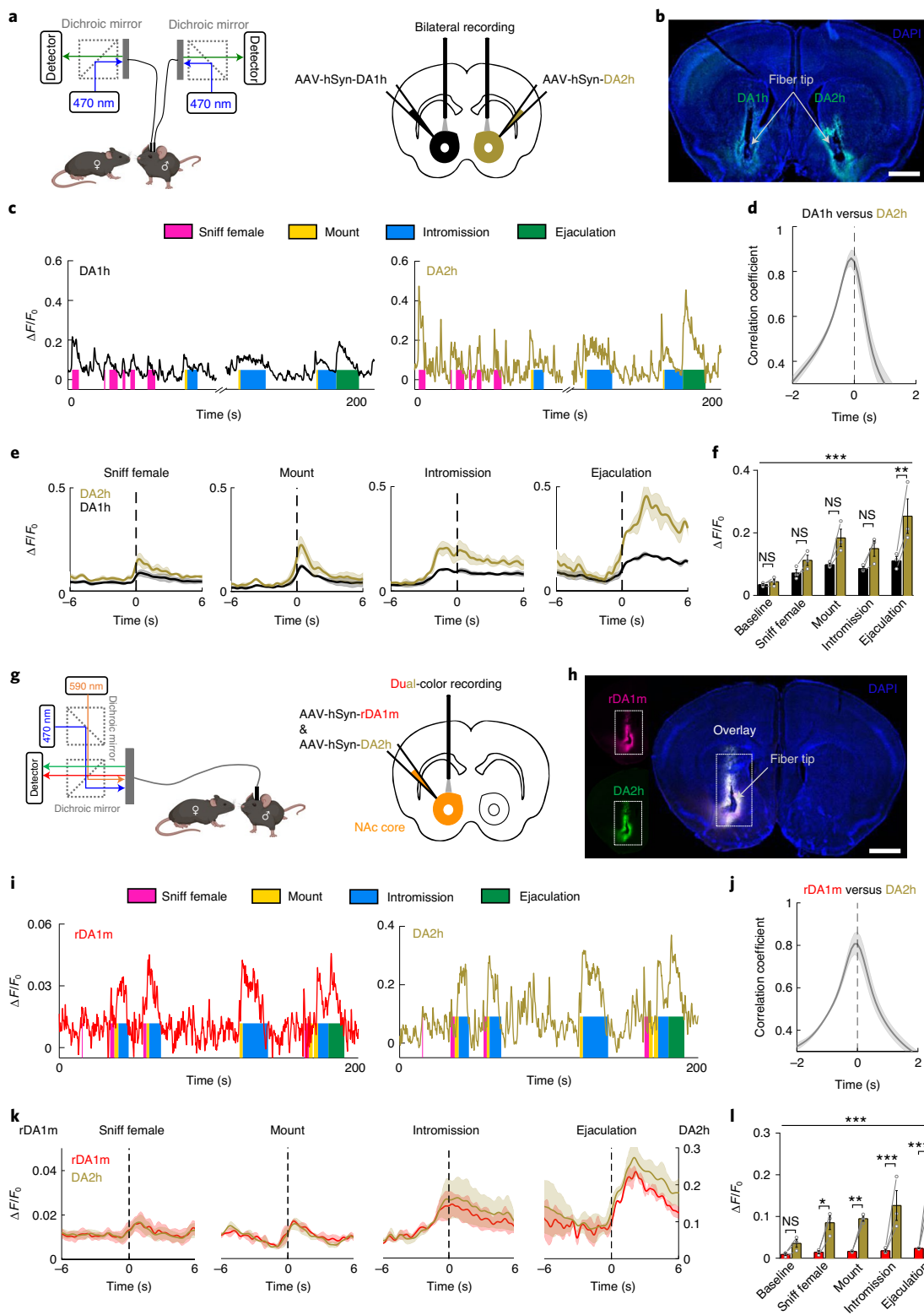


**Fig. 6 | GRAB<sub>DA</sub> sensors can be used to measure dopaminergic activity in the mouse NAc during sexual behavior.** **a**, Schematic illustration depicting the experimental strategy for panels **b–f**. **b**, Representative image showing the expression of DA1h and DA2h in opposite hemispheres. Similar results were observed for three mice. Scale bar, 1 mm. **c**, Representative traces of DA1h and DA2h  $\Delta F/F_0$  measured during the indicated stages of mating. Similar results were observed for three mice. **d**, The time shift correlation coefficient between the DA1h and DA2h signals.  $n = 3$  mice. **e**, Average poststimulus histograms aligned to the onset of the indicated mating events.  $n = 3$  mice. **f**, Group summary of  $\Delta F/F_0$  measured for DA1h and DA2h during the indicated mating events.  $n = 3$  mice.  $F_{4,16} = 15.43$ ,  $P = 2.0 \times 10^{-5}$  for row factor and  $F_{1,4} = 10.72$ ,  $P = 0.0307$  for column factor by two-way ANOVA. Bonferroni's multiple comparisons tests were performed between groups,  $P > 0.99$ ,  $P > 0.99$ ,  $P = 0.0732$ ,  $P = 0.2993$ ,  $P = 0.0013$ . **g**, Schematic illustration depicting the experimental strategy for panels **h–l**. **h**, Representative images showing the colocalized expression of rDA1m and DA2h. Similar results were observed for three mice. Scale bar, 1 mm. **i**, Representative traces of rDA1m and DA2h  $\Delta F/F_0$  measured during the indicated stages of mating. Similar results were observed for three mice. **j**, The time shift correlation coefficient between the rDA1m and DA2h signals.  $n = 3$  mice. **k**, Average poststimulus histograms aligned to the onset of the indicated mating events.  $n = 3$  mice. **l**, Group summary of the  $\Delta F/F_0$  measured for rDA1m and DA2h during the indicated mating events.  $n = 3$  mice.  $F_{4,16} = 8.613$ ,  $P = 0.0007$  for row factor and  $F_{1,4} = 52.46$ ,  $P = 0.0019$  by two-way ANOVA. Bonferroni's multiple comparisons tests were performed between groups,  $P > 0.99$ ,  $P = 0.0208$ ,  $P = 0.0092$ ,  $P = 0.0004$ ,  $P = 2.0 \times 10^{-6}$ . Average traces shaded with  $\pm$ s.e.m. are shown in **d**, **e**, **j** and **k**. Data are presented as the mean  $\pm$  s.e.m. in **f** and **l**. \* $P < 0.05$ ; \*\* $P < 0.01$ ; \*\*\* $P < 0.001$ .

high-affinity and medium-affinity versions provides the opportunity to probe DA dynamics over a broad range of concentrations.

The on rate of sensors can be the rate-limiting step to detect the release of DA upon physiologically relevant stimuli. Our sensors show fast kinetics that enable them to report subsecond events. The  $\tau_{\text{on}}$  values measured in cultured cells, brain slices, *Drosophila* and mice are within 80 ms, 150 ms, 40 ms and 120 ms, respectively. We note that the  $\tau_{\text{on}}$  values measured in brain slices and mice are overestimates considering the time needed for the stimulation to release DA. The  $\tau_{\text{off}}$  values measured in vivo in *Drosophila* and mice are within 280 ms and 610 ms, respectively. We note that these measured values depend on both the off kinetics of sensors and the speed of DA clearance. There is generally a tradeoff between SNR and off kinetics. Sensors with slower off kinetics have the advantage of prolonged photon collection, which contributes to a higher SNR. Our medium-affinity sensors can be used when faster off kinetics are required.

Our *Drosophila* in vivo imaging results demonstrate that the expression of GRAB<sub>DA</sub> sensors has no substantial effect on the body-shock-evoked cAMP signal and the odor-evoked calcium signal, which are the downstream signaling events of *Drosophila* endogenous DA receptors<sup>44,45</sup>. This suggests that DA buffering by the sensors in the extracellular space does lead to minimal perturbation to the endogenous cell physiology. Any residual buffering effect can be partially relieved by adjusting the expression level of the sensor, and by future improvements in the brightness and response of sensors.

Finally, the GRAB-based sensor strategy can be applied to creating genetically encoded sensors based on a wide range of G-protein-coupled receptors<sup>11,46–48</sup>, leading to a robust and versatile multi-color toolbox for creating comprehensive functional maps of neurochemical activity.

## Online content

Any methods, additional references, Nature Research reporting summaries, source data, extended data, supplementary information, acknowledgements, peer review information; details of author contributions and competing interests; and statements of data and code availability are available at <https://doi.org/10.1038/s41592-020-00981-9>.

Received: 30 March 2020; Accepted: 15 September 2020;  
Published: 21 October 2020

## References

- Björklund, A. & Dunnett, S. B. Dopamine neuron systems in the brain: an update. *Trends Neurosci.* **30**, 194–202 (2007).
- Wise, R. A. Dopamine, learning and motivation. *Nat. Rev. Neurosci.* **5**, 483–494 (2004).

- Klein, M. O. et al. Dopamine: functions, signaling, and association with neurological diseases. *Cell. Mol. Neurobiol.* **39**, 31–59 (2019).
- Tidey, J. W. & Miczek, K. A. Social defeat stress selectively alters mesocorticolimbic dopamine release: an in vivo microdialysis study. *Brain Res.* **721**, 140–149 (1996).
- Robinson, D. L., Venton, B. J., Heien, M. L. & Wightman, R. M. Detecting subsecond dopamine release with fast-scan cyclic voltammetry in vivo. *Clin. Chem.* **49**, 1763–1773 (2003).
- Muller, A., Joseph, V., Slesinger, P. A. & Kleinfeld, D. Cell-based reporters reveal in vivo dynamics of dopamine and norepinephrine release in murine cortex. *Nat. Methods* **11**, 1245–1252 (2014).
- Inagaki, H. K. et al. Visualizing neuromodulation in vivo: TANGO-mapping of dopamine signaling reveals appetite control of sugar sensing. *Cell* **148**, 583–595 (2012).
- Lee, D. et al. Temporally precise labeling and control of neuromodulatory circuits in the mammalian brain. *Nat. Methods* **14**, 495–503 (2017).
- Kruss, S. et al. High-resolution imaging of cellular dopamine efflux using a fluorescent nanosensor array. *Proc. Natl Acad. Sci. USA* **114**, 1789–1794 (2017).
- Beyene, A. G. et al. Imaging striatal dopamine release using a nongenetically encoded near infrared fluorescent catecholamine nanosensor. *Sci. Adv.* **5**, eaaw3108 (2019).
- Sun, F. et al. A genetically encoded fluorescent sensor enables rapid and specific detection of dopamine in flies, fish, and mice. *Cell* **174**, 481–496.e9 (2018).
- Patriarchi, T. et al. Ultrafast neuronal imaging of dopamine dynamics with designed genetically encoded sensors. *Science* **360**, 6396 (2018).
- Tanaka, M., Sun, F., Li, Y. & Mooney, R. A mesocortical dopamine circuit enables the cultural transmission of vocal behaviour. *Nature* **563**, 117–120 (2018).
- Zhou, M. et al. Suppression of GABAergic neurons through D2-like receptor secures efficient conditioning in *Drosophila* aversive olfactory learning. *Proc. Natl Acad. Sci. USA* **116**, 5118–5125 (2019).
- Handler, A. et al. Distinct dopamine receptor pathways underlie the temporal sensitivity of associative learning. *Cell* **178**, 60–75.e19 (2019).
- Shu, X. et al. Mammalian expression of infrared fluorescent proteins engineered from a bacterial phytochrome. *Science* **324**, 804–807 (2009).
- Alford, S. C., Wu, J., Zhao, Y., Campbell, R. E. & Knöpfel, T. Optogenetic reporters. *Biol. Cell* **105**, 14–29 (2013).
- Zhao, Y. et al. An expanded palette of genetically encoded Ca<sup>2+</sup> indicators. *Science* **333**, 1888–1891 (2011).
- Bindels, D. S. et al. mScarlet: a bright monomeric red fluorescent protein for cellular imaging. *Nat. Methods* **14**, 53–56 (2017).
- Feng, S. et al. Improved split fluorescent proteins for endogenous protein labeling. *Nat. Commun.* **8**, 370 (2017).
- Shemiakina, I. I. et al. A monomeric red fluorescent protein with low cytotoxicity. *Nat. Commun.* **3**, 1204 (2012).
- Sung, Y. M., Wilkins, A. D., Rodriguez, G. J., Wensel, T. G. & Lichtarge, O. Intramolecular allosteric communication in dopamine D2 receptor revealed by evolutionary amino acid covariation. *Proc. Natl Acad. Sci. USA* **113**, 3539–3544 (2016).
- Chien, E. Y. et al. Structure of the human dopamine D3 receptor in complex with a D2/D3 selective antagonist. *Science* **330**, 1091–1095 (2010).
- Wu, J. et al. Improved orange and red Ca<sup>2+</sup> indicators and photophysical considerations for optogenetic applications. *ACS Chem. Neurosci.* **4**, 963–972 (2013).
- Dana, H. et al. Sensitive red protein calcium indicators for imaging neural activity. *eLife* **5**, <https://doi.org/10.7554/eLife.12727> (2016).

26. Pedelacq, J. D., Cabantous, S., Tran, T., Terwilliger, T. C. & Waldo, G. S. Engineering and characterization of a superfolder green fluorescent protein. *Nat. Biotechnol.* **24**, 79–88 (2006).
27. St-Pierre, F. et al. High-fidelity optical reporting of neuronal electrical activity with an ultrafast fluorescent voltage sensor. *Nat. Neurosci.* **17**, 884–889 (2014).
28. Bajar, B. T. et al. Improving brightness and photostability of green and red fluorescent proteins for live cell imaging and FRET reporting. *Sci. Rep.* **6**, 20889 (2016).
29. Baird, G. S., Zacharias, D. A. & Tsien, R. Y. Circular permutation and receptor insertion within green fluorescent proteins. *Proc. Natl Acad. Sci. USA* **96**, 11241–11246 (1999).
30. Wan, Q. et al. Mini G protein probes for active G protein-coupled receptors (GPCRs) in live cells. *J. Biol. Chem.* **293**, 7466–7473 (2018).
31. Kroeze, W. K. et al. PRESTO-Tango as an open-source resource for interrogation of the druggable human GPCRome. *Nat. Struct. Mol. Biol.* **22**, 362 (2015).
32. Broussard, G. J. et al. In vivo measurement of afferent activity with axon-specific calcium imaging. *Nat. Neurosci.* **21**, 1272–1280 (2018).
33. Schwaerzel, M. et al. Dopamine and octopamine differentiate between aversive and appetitive olfactory memories in *Drosophila*. *J. Neurosci.* **23**, 10495–10502 (2003).
34. Kim, Y.-C., Lee, H.-G. & Han, K.-A. D1 dopamine receptor dDA1 is required in the mushroom body neurons for aversive and appetitive learning in *Drosophila*. *J. Neurosci.* **27**, 7640–7647 (2007).
35. Schroll, C. et al. Light-induced activation of distinct modulatory neurons triggers appetitive or aversive learning in *Drosophila* larvae. *Curr. Biol.* **16**, 1741–1747 (2006).
36. Claridge-Chang, A. et al. Writing memories with light-addressable reinforcement circuitry. *Cell* **139**, 405–415 (2009).
37. Tanaka, N. K., Tanimoto, H. & Ito, K. Neuronal assemblies of the *Drosophila* mushroom body. *J. Comp. Neurol.* **508**, 711–755 (2008).
38. Mao, Z. & Davis, R. L. Eight different types of dopaminergic neurons innervate the *Drosophila* mushroom body neuropil: anatomical and physiological heterogeneity. *Front. Neural Circuits* **3**, 5 (2009).
39. Aso, Y. et al. The neuronal architecture of the mushroom body provides a logic for associative learning. *eLife* **3**, e04577 (2014).
40. Klapoetke, N. C. et al. Independent optical excitation of distinct neural populations. *Nat. Methods* **11**, 338–346 (2014).
41. Harada, K. et al. Red fluorescent protein-based cAMP indicator applicable to optogenetics and in vivo imaging. *Sci. Rep.* **7**, 7351 (2017).
42. Akerboom, J. et al. Optimization of a GCaMP calcium indicator for neural activity imaging. *J. Neurosci.* **32**, 13819–13840 (2012).
43. Yizhar, O. et al. Neocortical excitation/inhibition balance in information processing and social dysfunction. *Nature* **477**, 171–178 (2011).
44. Sugamori, K. S., Demchyshyn, L. L., McConkey, E., Forte, M. A. & Niznik, H. B. A primordial dopamine D1-like adenylyl cyclase-linked receptor from *Drosophila melanogaster* displaying poor affinity for benzazepines. *FEBS Lett.* **362**, 131–138 (1995).
45. Himmelreich, S. et al. Dopamine receptor DAMB signals via Gq to mediate forgetting in *Drosophila*. *Cell Rep.* **21**, 2074–2081 (2017).
46. Jing, M. et al. A genetically encoded fluorescent acetylcholine indicator for in vitro and in vivo studies. *Nat. Biotechnol.* **36**, 726–737 (2018).
47. Jing, M. et al. An optimized acetylcholine sensor for monitoring in vivo cholinergic activity. *Nat. Methods* <https://doi.org/10.1038/s41592-020-0953-2> (2020).
48. Feng, J. et al. A genetically encoded fluorescent sensor for rapid and specific in vivo detection of norepinephrine. *Neuron* **102**, 745–761.e8 (2019).

**Publisher's note** Springer Nature remains neutral with regard to jurisdictional claims in published maps and institutional affiliations.

© The Author(s), under exclusive licence to Springer Nature America, Inc. 2020

## Methods

**Animals.** Male and female postnatal day (P)0 Sprague-Dawley rats (Beijing Vital River Laboratory) and adult (P42–90) wild-type C57BL/6N (Beijing Vital River Laboratory), wild-type C57BL/6N (Charles River Laboratories), DAT-IRES-Cre (Jackson Laboratory, stock number 06660), *Drd1-cre* (MMRRC\_036916-UCD; Extended Data Fig. 9) and *Drd1-cre* (MMRRC\_030989-UCD; Extended Data Fig. 10a–c) mice were used in this study. Mice were housed at 18–23 °C with 40–60% humidity under a 12-h/12-h light/dark cycle, with food and water available ad libitum. All procedures for animal surgery, maintenance and behavior were performed using protocols that were approved by the respective animal care and use committees at Peking University, New York University and the US National Institutes of Health.

The transgenic *Drosophila* lines UAS-rDA1m, UAS-rDA-mut, UAS-DA2m, UAS-dLight1.3b, LexAOp-DA2m and UAS-Pink-Flamingo were generated using Phi-C31-directed integration into *atp40* or VK00005 at the Core Facility of *Drosophila* Resource and Technology, Shanghai Institute of Biochemistry and Cell Biology, Chinese Academy of Sciences. The following *Drosophila* lines were also used in this study: UAS-DA1m (Bloomington *Drosophila* Stock Center (BDSC): 80047), R13F02-Gal4 (BDSC: 48571), R13F02-LexA (BDSC: 52460), 30y-Gal4 and TH-Gal4-3p3-RFP (ref. 49) (all gifts from Yi Rao, Peking University, Beijing); MB312C-Gal4 (Fly light: 2135360); MB315C-Gal4 (Fly light: 2135363); UAS-CsChrimson-mCherry (a gift from Chuan Zhou, Institute of Zoology, Chinese Academy of Sciences, Beijing); and UAS-GCaMP5G (BDSC: 42038). The flies were raised on standard cornmeal-yeast medium at 25 °C and 70% relative humidity under a 12-h/12-h light/dark cycle. Adult female flies within 2 weeks after eclosion were used for fluorescence imaging.

**Molecular biology.** DNA fragments were generated using PCR amplification with primers (TSINGKE Biological Technology) containing 30-base-pair overlap. The fragments were then assembled into plasmids using Gibson assembly<sup>50</sup>. All plasmid sequences were verified using Sanger sequencing (TSINGKE Biological Technology). For characterization in HEK293T cells, the genes expressing the red and green DA sensors were cloned into the pDisplay vector, with an IgK leader sequence inserted upstream of the sensor gene. The IRES-EGFP-CAAX gene (for red DA sensors) or IRES-mCherry-CAAX gene (for green DA sensors) was attached downstream of the sensor gene and was used as a membrane marker and to calibrate the fluorescence signal intensity. Site-directed mutagenesis was performed using primers containing randomized NNB codons (48 codons in total, encoding 20 possible amino acids) or defined codons on the target sites. For characterization in cultured neurons, the sensor genes were cloned into the pAAV vector under the control of the human synapsin promoter (hSyn). To generate stable cell lines expressing wild-type D<sub>2</sub>R, rDA1h or DA2h, we generated a vector called pPacific, containing various elements, including 3' terminal repeat, the myc tag gene, a 2A self-cleaving sequence, the mCherry gene, the puromycin gene and 5' terminal repeat; the genes were then cloned into the pPacific vector using Gibson assembly. Two mutations (S103P and S509G) were introduced in pCS7-PiggyBAC (ViewSolid Biotech) to generate a hyperactive piggyBac transposase<sup>51</sup> for generating stable cell lines. For the TANGO assay, the wild-type D<sub>2</sub>R, rDA1h or DA2h genes were cloned into the pTango vector<sup>51</sup>. For the luciferase complementation assay, we replaced the β<sub>2</sub>AR gene in the β<sub>2</sub>AR-Smbit construct<sup>50</sup> with the wild-type D<sub>2</sub>R, rDA1h or DA2h genes. To generate transgenic *Drosophila* lines, the respective sensor genes were cloned into the pJRC28 for UAS lines and modified pJRC19 (the SV40 terminator was replaced by the terminator from the AcNPV p10 gene) for LexAop lines, which were then used for Phi-C31 site-specific insertion.

**Preparation and fluorescence imaging of cultured cells.** HEK293T cells were cultured in DMEM (Gibco) supplemented with 10% (v/v) fetal bovine serum (Gibco) and 1% penicillin-streptomycin (Gibco) at 37 °C in 5% CO<sub>2</sub>. The cells were plated on 96-well plates or 12-mm glass coverslips in 24-well plates and grown to 60% confluence for transfection. For transfection, the cells were incubated in a mixture containing 1 μg of DNA and 3 μg of polyethylenimine for 6 h. Fluorescence imaging was performed 24–48 h after transfection. Rat cortical neurons were prepared from P0 Sprague-Dawley rat pups (Beijing Vital River Laboratory). In brief, cortical neurons were dissociated from dissected rat brains in 0.25% Trypsin-EDTA (Gibco), plated on 12-mm glass coverslips coated with poly-D-lysine (Sigma-Aldrich) and cultured in Neurobasal medium (Gibco) containing 2% B-27 supplement (Gibco), 1% GlutaMAX (Gibco) and 1% penicillin-streptomycin (Gibco) at 37 °C in 5% CO<sub>2</sub>. The neurons were transfected with an AAV expressing rDA1m, rDA1h, DA2m, DA2h or dLight1.1 (Vigene Biosciences) after 7–9 d in culture, and fluorescence imaging was performed 3–7 d after transfection.

Cultured cells were imaged using an inverted Ti-E A1 confocal microscope (Nikon) and the Opera Phenix high-content screening system (PerkinElmer). The confocal microscope was equipped with a ×40/1.35 numerical aperture oil-immersion objective, a 488-nm laser and a 561-nm laser. During fluorescence imaging, the cells were either bathed or perfused in a chamber containing Tyrode's solution consisting of (in mM): 150 NaCl, 4 KCl, 2 MgCl<sub>2</sub>, 2 CaCl<sub>2</sub>, 10 HEPES and 10 glucose (pH 7.4). Solutions containing various concentrations of DA (Sigma-Aldrich) and/or 1 μM Halo (Tocris), SCH-23390 (Tocris), Etic (Tocris),

L-DOPA (Abcam), 5-HT (Tocris), histamine (Tocris), Glu (Sigma-Aldrich), GABA (Tocris), Ado (Tocris), ACh (Solarbio), norepinephrine (Tocris), Tyr (Sigma-Aldrich) or Oct (Tocris) were delivered via a custom-made perfusion system or via bath application. Between experiments, the chamber was thoroughly cleaned with 75% ethanol, 3% hydrogen peroxide and Tyrode's solution. GFP fluorescence was collected using a 525/50-nm emission filter, and RFP fluorescence was collected using a 595/50-nm emission filter. To measure the response kinetics, a glass pipette filled with DA or Halo was positioned close to the GRAB<sub>DA</sub>-expressing cells, and the fluorescence signals were measured using confocal line-scanning (scanning speed at 1,280 Hz). To measure the on rate, 100 μM DA in a glass pipette was applied. To measure the off rate, 1 mM Halo in a glass pipette was applied to the sensor-expressing cells bathed in DA (10 μM DA for rDA1m and DA2m, 1 μM DA for rDA1h and DA2h). Photostability was measured under one-photon illumination (confocal microscopy) using a 488-nm laser with laser power of 350 μW and intensity of ~2.2 W cm<sup>-2</sup>, and a 561-nm laser with laser power of 790 μW and intensity of ~4.9 W cm<sup>-2</sup>; and under two-photon illumination using a 920-nm laser with laser power of 27.5 mW and intensity of ~13 W cm<sup>-2</sup>. Photobleaching was applied to the entire sensor-expressing HEK293T cell at an area of ~200 μm<sup>2</sup>. Blue-light-mediated photoactivation was measured using a 488-nm laser with laser power of 350 μW and intensity of ~0.7 W cm<sup>-2</sup>. The Opera Phenix high-content screening system was equipped with a ×60/1.15 numerical aperture water-immersion objective, a 488-nm laser and a 561-nm laser. GFP fluorescence was collected using a 525/50-nm emission filter, and RFP fluorescence was collected using a 600/30-nm emission filter. Where indicated, the culture medium was replaced with 100 μl of Tyrode's solution containing various concentrations of the indicated drugs. The red and green sensors' fluorescence intensity was calibrated using EGFP and mCherry, respectively.

**Spectra measurements.** HEK293T cells stably expressing rDA1m, rDA1h or DA2h were collected and transferred to a 96-well plate in the absence or presence of 100 μM DA, and excitation and emission spectra were measured at 5-nm increments using a Safire2 multi-mode plate reader (Tecan).

**Luciferase complementation assay.** The luciferase complementation assay was performed as previously described<sup>50</sup>. In brief, 24–48 h after transfection, HEK293T cells expressing rDA1h with LgBit-mGi, DA2h with LgBit-mGi or LgBit-mGi alone were washed in PBS, collected by trituration and transferred to 96-well plates. DA at various concentrations (ranging from 1 nM to 100 μM) was applied to the cells, and furimazine (NanoLuc Luciferase Assay, Promega) was then applied to a final concentration of 5 μM, after which luminescence was measured using a Victor X5 multi-label plate reader (PerkinElmer).

**TANGO assay.** DA was applied at various concentrations (ranging from 0.1 nM to 10 μM) to a reporter cell line stably expressing a tTA-dependent luciferase reporter and a β-arrestin2-TEV fusion gene<sup>51</sup> transfected to express wild-type D<sub>2</sub>R, rDA1h or DA2h. The cells were then cultured for 12 h to allow for luciferase expression. Bright-Glo (Fluc Luciferase Assay System, Promega) was then applied to a final concentration of 5 μM, and luminescence was measured using a VICTOR X5 multi-label plate reader (PerkinElmer).

**GTPγS treatment.** The culture medium of HEK293T cells expressing rDA1h or DA2h was replaced by 100 μl of Tyrode's solution before experiments. For the group with GTPγS treatment, cells were subsequently incubated with 50 μg ml<sup>-1</sup> digitonin (Sigma-Aldrich) for 5 min to permeabilize the cell membrane and washed twice with 100 μl of Tyrode's solution. The cells were then incubated with Tyrode's solution containing 100 μM GTPγS (Sigma-Aldrich) for 10 min. Various concentrations of DA (ranging from 0.01 nM to 100 μM) were applied. The fluorescence signals were measured using the Opera Phenix high-content screening system (PerkinElmer) mentioned above.

**Preparation and fluorescence imaging of acute brain slices.** Wild-type male and female adult (P42–56) C57BL/6N mice were anesthetized with an intraperitoneal (i.p.) injection of 2,2,2-tribromoethanol (Avertin, 500 mg kg<sup>-1</sup> body weight, Sigma-Aldrich), and then placed in a stereotaxic frame for AAV injection using a microsyringe pump (Nanoliter 2000 Injector, WPI). In Fig. 3a–e, AAVs expressing hSyn-rDA1m, hSyn-rDA1h or hSyn-DA2m (Vigene Biosciences) were injected (400 nl per injection site) into the NAc using the following coordinates: anterior–posterior (AP), +1.4 mm relative to bregma; medial–lateral (ML), ±1.2 mm relative to bregma; depth, 4.0 mm from the dura. In Fig. 3f–k, the AAV expressing hSyn-rDA1m (Vigene Biosciences) was injected (400 nl per injection site) into the NAc using the coordinates listed above, and the AAV expressing hSyn-axon-GCaMP6s (BrainVTA) was injected (400 nl per injection site) into the ventral tegmental area using the following coordinates: AP, –3.2 mm relative to bregma; ML, ±0.5 mm relative to bregma; depth, 4.1 mm from the dura.

At 2 weeks after virus injection, the mice were anesthetized with an i.p. injection of Avertin (500 mg per kg body weight) and perfused with ice-cold oxygenated slicing buffer containing (in mM): 110 choline-Cl, 2.5 KCl, 1 NaH<sub>2</sub>PO<sub>4</sub>, 25 NaHCO<sub>3</sub>, 7 MgCl<sub>2</sub>, 25 glucose and 0.5 CaCl<sub>2</sub>. The brains were immediately removed and placed in ice-cold oxygenated slicing buffer. The



brains were sectioned into 300- $\mu\text{m}$ -thick slices using a VT1200 vibratome (Leica), and the slices were incubated at 34 °C for at least 40 min in oxygenated artificial cerebrospinal fluid containing (in mM): 125 NaCl, 2.5 KCl, 1 NaH<sub>2</sub>PO<sub>4</sub>, 25 NaHCO<sub>3</sub>, 1.3 MgCl<sub>2</sub>, 25 glucose and 2 CaCl<sub>2</sub>. For fluorescence imaging, the slices were transferred to an imaging chamber and placed under an FV1000MPE two-photon microscope (Olympus) equipped with a  $\times 25/1.05$  numerical aperture water-immersion objective and a mode-locked Mai Tai Ti:Sapphire laser (Spectra-Physics). A 950-nm laser was used to excite rDA1m and rDA1h, and fluorescence was collected using a 575–630-nm filter. A 920-nm laser was used to excite DA2m, and fluorescence was collected using a 495–540-nm filter. For electrical stimulation, a bipolar electrode (catalog no. WE30031.0A3, MicroProbes for Life Science) was positioned near the core of the NAc using fluorescence guidance. Fluorescence imaging and electrical stimulation were synchronized using an Arduino board with custom-written programs. All images collected during electrical stimulation were recorded at a frame rate of 0.1482 s per frame with 128  $\times$  96 pixels per frame. The stimulation voltage was 4–6 V, and the duration of each stimulus was 1 ms. Drugs were applied to the imaging chamber by perfusion at a flow rate at 4 ml min<sup>-1</sup>.

**Fluorescence imaging of transgenic flies.** Adult female flies (within 2 weeks after eclosion) were used for fluorescence imaging. The fly dissection procedure and the recipe for adult hemolymph-like solution, as well as the two-photon microscopy setup for odor, body shock and DA perfusion, have been described previously<sup>11</sup>. A 575–630-nm filter and a 575–630-nm filter were used to collect the red and green fluorescence, respectively. A 950-nm laser was used to excite rDA1m and Pink-Flamindo, a 930-nm laser was used to excite DA2m and dLight1.3b, a 950-nm laser was used for DA2m and Pink-Flamindo dual-color imaging and a 1,000-nm laser was used for GCaMP5 and rDA1m dual-color imaging. Linear unmixing was adopted to process dual-color imaging results. For optogenetic stimulation, a 200-mW 635-nm laser (Changchun Liangli Photoelectricity) was used to deliver light to the fly brain via an optical fiber. An Arduino board with custom-written programs was used to synchronize the stimulation and fluorescence imaging. The sampling rate during odorant stimulation, electrical stimulation, body shock and DA perfusion was 6.7 Hz, 12 Hz, 6.7 Hz and 1 Hz, respectively.

**Fiber photometry recording of nigrostriatal DA release in freely moving mice.** Adult (P42–56) male and female DAT-DRE-Cre mice (Jackson Laboratory, stock number 06660) and Drd1-cre mice (MMRRC\_036916-UCD) were anesthetized with isoflurane and placed in a stereotaxic frame for AAV injection. AAVs expressing hSyn-rDA1m, hSyn-rDA1h, hSyn-rDA-mut, hSyn-DA2m or hSyn-DA2h (Vigene Biosciences) as well as hSyn-EGFP (Addgene, catalog no. 50465) or hSyn-tdTomato (a gift from J. L. Yaker's laboratory, National Institute of Environmental Health Sciences) were injected (1  $\mu\text{l}$  per site) into the dorsal striatum using the following coordinates: AP, -0.5 mm relative to bregma; ML,  $\pm 2.4$  mm relative to bregma; depth, 2.2 mm from the dura. The AAV expressing Efl $\alpha$ -DIO-C1V1-YFP (NIEHS Viral Vector Core) was injected (500 nl per site) into the SNc using the following coordinates: AP, -3.1 mm relative to bregma; ML,  $\pm 1.5$  mm relative to bregma; depth, 4.0 mm from the dura. For the dual-color recording in Extended Data Fig. 9, AAVs expressing hSyn-DIO-NES-jRGECO1a (ref. <sup>52</sup>) (NIEHS Viral Vector Core) and hSyn-DA2m (Vigene Biosciences) were injected at a 9:1 ratio with a total volume of 1  $\mu\text{l}$ , using the following coordinates: AP, +0.5 mm relative to bregma; ML,  $\pm 1.8$  mm relative to bregma; depth, 2.75 mm from the dura. Optical fibers (105- $\mu\text{m}$  core/125- $\mu\text{m}$  cladding) were implanted in the dorsal striatum and SNc 4 weeks after AAV injection. Fiber photometry recording in the dorsal striatum was performed using a 488-nm laser at 50  $\mu\text{W}$  for DA2m and DA2h, and a 488-nm laser at 1  $\mu\text{W}$  and a 561-nm laser at 50  $\mu\text{W}$  for rDA1m, rDA1h, rDA-mut and jRGECO1a. C1V1 in the SNc was stimulated using a 561-nm laser at 9.9 mW. Spectral data were acquired by the software OceanView (Ocean Insight). The measured emission spectra were fitted using a linear unmixing algorithm (<https://www.niehs.nih.gov/research/atniehs/labs/lm/pi/iv/tools/index.cfm>). To evoke C1V1-mediated DA release, pulse trains (10-ms pulses at 20 Hz for 1 s) were delivered to the SNc using a 561-nm laser at 9.9 mW. To avoid signal decay, the excitation lasers were controlled using an optical shutter (Thorlabs) in which the shutter was turned on 10 s before the 561-nm pulse trains and turned off 35 s after stimulation. To test the effects of methylphenidate and eticlopride on C1V1-evoked responses, five optical stimulation trains were given with an interval of 1 min (for green GRAB<sub>DA</sub> sensors) or 2 min (for red GRAB<sub>DA</sub> sensors) between each train to obtain baseline responses. Then, 10 mg kg<sup>-1</sup> methylphenidate was administered by i.p. injection. At 10 min after the i.p. injection, five more optical stimulation trains were delivered to record the C1V1-evoked responses under the influence of methylphenidate. Finally, an i.p. injection of 1 mg kg<sup>-1</sup> eticlopride was given and five more trials of optical stimulations were delivered 10 min after the injection to record C1V1-evoked responses under eticlopride.

**Fiber photometry recording of DA dynamics in the NAc during sexual behavior.** Adult (P60–90) wild-type male C57BL/6N mice (Charles River Laboratories) and Drd1-cre male mice (MMRRC\_030989-UCD) were anesthetized with isoflurane and placed in a stereotaxic frame for AAV injection. For Fig. 6, AAVs

expressing hSyn-rDA1m, hSyn-DA1h or hSyn-DA2h (Vigene Biosciences) were injected (80–140 nl per site) into the NAc using the following coordinates: AP, +0.98 mm relative to bregma; ML,  $\pm 1.2$  mm relative to bregma; depth, 4.6 mm from the dura. For the coexpression of rDA1m and DA2h in Fig. 6g–i, AAVs expressing hSyn-rDA1m and hSyn-DA2h were injected at a 1:1 ratio. For the bilateral recording in Extended Data Fig. 10a–c, AAV expressing hSyn-DIO-DA2h was injected bilaterally using the same coordinates described above. After AAV injection, optical fibers (400- $\mu\text{m}$  diameter) were implanted in the NAc, and fiber photometry recording was performed 2 weeks after AAV injection. The setups for bilateral recording and dual-color recording are shown in Fig. 6a,g, respectively. In brief, a 311-Hz 472/30-nm filtered light-emitting diode (Thorlabs) at 30  $\mu\text{W}$  was used to excite DA1h and DA2h, and a 400-Hz 590/20-nm filtered light-emitting diode (Thorlabs) at 30  $\mu\text{W}$  was used to excite rDA1m. A 535/50-nm filter was used to collect the fluorescence signal from DA1h and DA2h, and a 524/628–25-nm dual-band bandpass filter was used to collect the fluorescence signal from rDA1m and DA2h during the dual-color recording. The signals were recorded using a real-time processor (RZ5, TDT) and extracted in real time using a custom TDT program. Animal behaviors were recorded using the commercial video acquisition software StreamPix 5 (Norpix). Behavioral annotation and tracking were performed using custom MATLAB codes (MATLAB R2019a, MathWorks). The various sexual behaviors are defined as previously described<sup>11</sup> following published conventions<sup>53</sup>. For immunofluorescence, the mice were anesthetized and then perfused with 4% paraformaldehyde. The brains were removed, fixed in 4% paraformaldehyde for 4 h and then cryoprotected in 20% (w/v) sucrose for 24 h. The brains were then embedded in tissue-freezing medium and sectioned into 60- $\mu\text{m}$ -thick slices using a CM1900 cryostat (Leica). rDA1m was immunostained using a rabbit anti-RFP antibody (1:1,000, Takara, catalog no. 632496) followed by a Cy3-conjugated donkey anti-rabbit secondary antibody (1:1,000, Jackson ImmunoResearch, catalog no. 113713). DA1h and DA2h were immunostained using a chicken anti-GFP antibody (1:1,000, Abcam, catalog no. ab13970) followed by an Alexa 488-conjugated donkey anti-chicken secondary antibody (1:1,000, Jackson ImmunoResearch, cat. no. 116967). The fluorescence images were acquired with a virtual slide microscope (Olympus, VS120).

**Quantification and statistical analysis.** Imaging data from cultured cells, acute brain slices and transgenic flies were processed using ImageJ 1.52p software (NIH). The fluorescence response ( $\Delta F/F_0$ ) was calculated using the formula  $(F - F_0)/F_0$ , in which  $F_0$  is the baseline fluorescence signal. The SNR was calculated as the peak response divided by the standard deviation of the baseline fluorescence fluctuation. The cross-correlation analyses were performed using NeuroExplorer 5 (Nex Technologies) and GraphPad Prism 7. Values with error bars indicate mean  $\pm$  s.e.m. The statistical analyses were performed using GraphPad Prism 7 and 8. Two-tailed Student's *t*-test, two-way analysis of variance (ANOVA) with Bonferroni's multiple comparisons test (Fig. 6f,i and Extended Data Fig. 10c,f) and one-way ANOVA with Tukey's multiple comparisons test (Extended Data Fig. 10h,j) were performed. \* $P < 0.05$ ; \*\* $P < 0.01$ ; \*\*\* $P < 0.001$ ; not significant (NS)  $P > 0.05$ . The exact *P* value is specified in the legends. The graphs were generated using OriginPro 9.1 (OriginLab) and GraphPad Prism 7 and 8.

**Reporting Summary.** Further information on research design is available in the Nature Research Reporting Summary linked to this article.

## Data availability

Plasmids for expressing the sensors used in this study and the sequences were available from Addgene ([https://www.addgene.org/Yulong\\_Li/](https://www.addgene.org/Yulong_Li/), catalog nos. 140553, 140554, 140555, 140556, 140557, 140558). Source data are provided with this paper.

## Code availability

The custom MATLAB codes and TDT programs are available from <https://github.com/pdollar/toolbox> and [https://github.com/bd125/GRAB\\_DA\\_Fig6\\_Code](https://github.com/bd125/GRAB_DA_Fig6_Code).

## References

- Deng, B. et al. Chemoconnectomics: mapping chemical transmission in *Drosophila*. *Neuron* **101**, 876–893. e874 (2019).
- Gibson, D. G. et al. Enzymatic assembly of DNA molecules up to several hundred kilobases. *Nat. Methods* **6**, 343–345 (2009).
- Yusa, K., Zhou, L., Li, M. A., Bradley, A. & Craig, N. L. A hyperactive piggyBac transposase for mammalian applications. *Proc. Natl Acad. Sci. USA* **108**, 1531–1536 (2011).
- Meng, C. et al. Spectrally resolved fiber photometry for multi-component analysis of brain circuits. *Neuron* **98**, 707–717.e4 (2018).
- Hull, E. M., Meisel, R. L. & Sachs, B. D. Male sexual behavior. in *Hormones, Brain and Behavior* pp. 3–137 (Academic, 2002).
- Ballesteros, J. A. & Weinstein, H. Integrated methods for the construction of three-dimensional models and computational probing of structure-function relations in G protein-coupled receptors. in *Methods in Neurosciences* Vol. 25 pp. 366–428 (Academic, 1995).

## Acknowledgements

This work was supported by the Beijing Municipal Science & Technology Commission (grant no. Z181100001318002), the Beijing Brain Initiative of Beijing Municipal Science & Technology Commission (grant no. Z181100001518004), Guangdong Grant 'Key Technologies for Treatment of Brain Disorders' (grant no. 2018B030332001), the General Program of the National Natural Science Foundation of China (project nos. 31671118, 31871087 and 31925017) and the NIH BRAIN Initiative (grant no. NS103558); and by grants from the Peking-Tsinghua Center for Life Sciences and the State Key Laboratory of Membrane Biology at Peking University School of Life Sciences to Y.L.; the NIH (grant nos. R01MH101377 and R21HD090563) and an Irma T. Hirschl Career Scientist Award to D.L.; and the Intramural Research Program of the US NIH/NIEHS (grant no. 1ZIAES103310) to G.C. We thank Y. Rao for sharing the two-photon microscope and X. Lei at PKU-CLS for providing support for the Opera Phenix high-content screening system.

## Author contributions

Y.L. supervised the study. F.S. and Y.L. designed the study. F.S., Y. Zhuo, Y. Zhang and C.Q. performed the experiments related to developing, optimizing and characterizing the sensors in cultured HEK293T cells and neurons with help from J.F. and H.D. F.S. and T.Q. performed the surgery and two-photon imaging experiments related to the

validation of the sensors in acute brain slices. J. Zeng, X.L., Y.W. and K.T. performed the two-photon imaging experiments in transgenic flies. J. Zhou performed the fiber photometry recordings during optogenetics in freely moving mice under the supervision of G.C. B.D. performed the fiber photometry recordings in the mouse NAc during sexual behavior under the supervision of D.L. All authors contributed to the data interpretation and analysis. F.S. and Y.L. wrote the manuscript with input from all authors.

## Competing interests

F.S. and Y. L. have filed patent applications whose value might be affected by this publication.

## Additional information

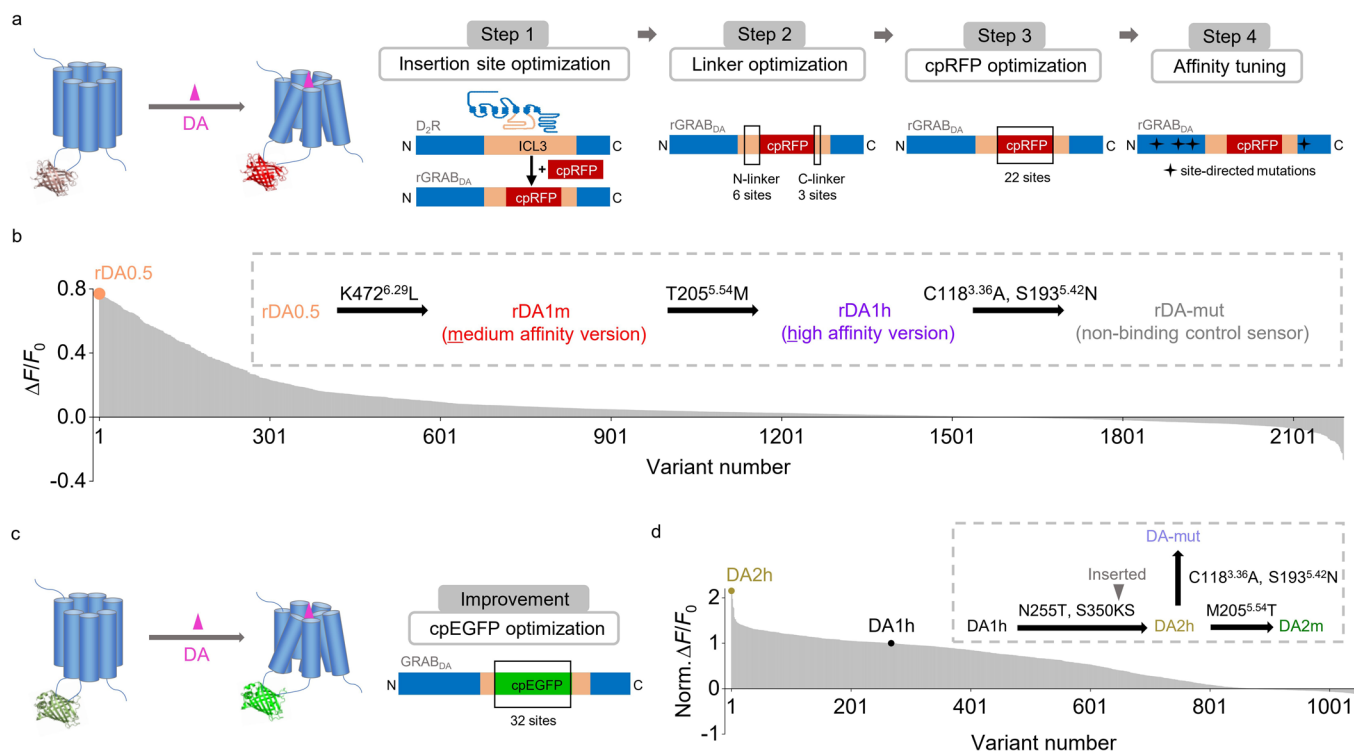
**Extended data** is available for this paper at <https://doi.org/10.1038/s41592-020-00981-9>.

**Supplementary information** is available for this paper at <https://doi.org/10.1038/s41592-020-00981-9>.

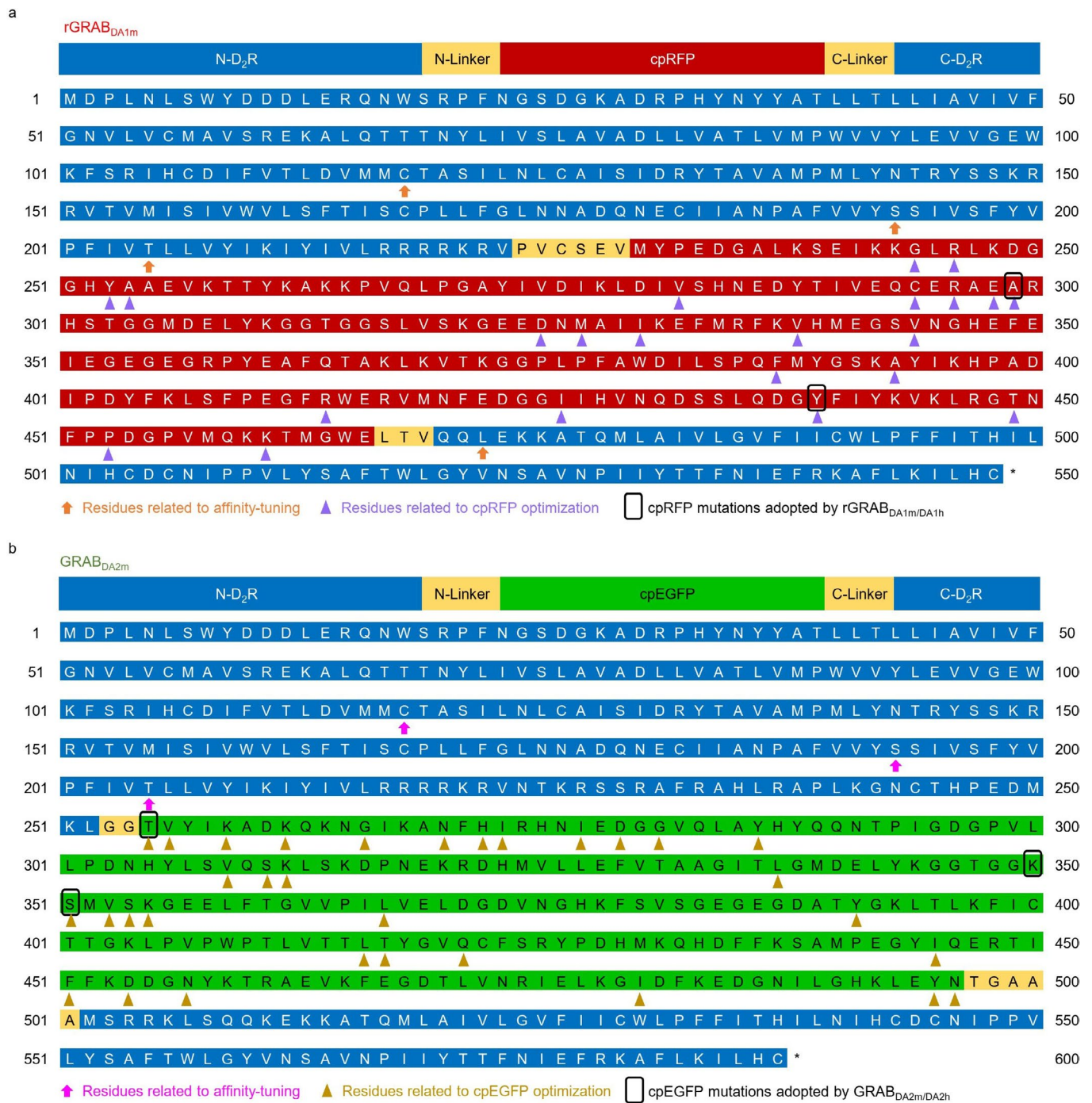
**Correspondence and requests for materials** should be addressed to D.L., G.C. or Y.L.

**Peer review information** Nina Vogt was the primary editor on this article and managed its editorial process and peer review in collaboration with the rest of the editorial team.

**Reprints and permissions information** is available at [www.nature.com/reprints](http://www.nature.com/reprints).

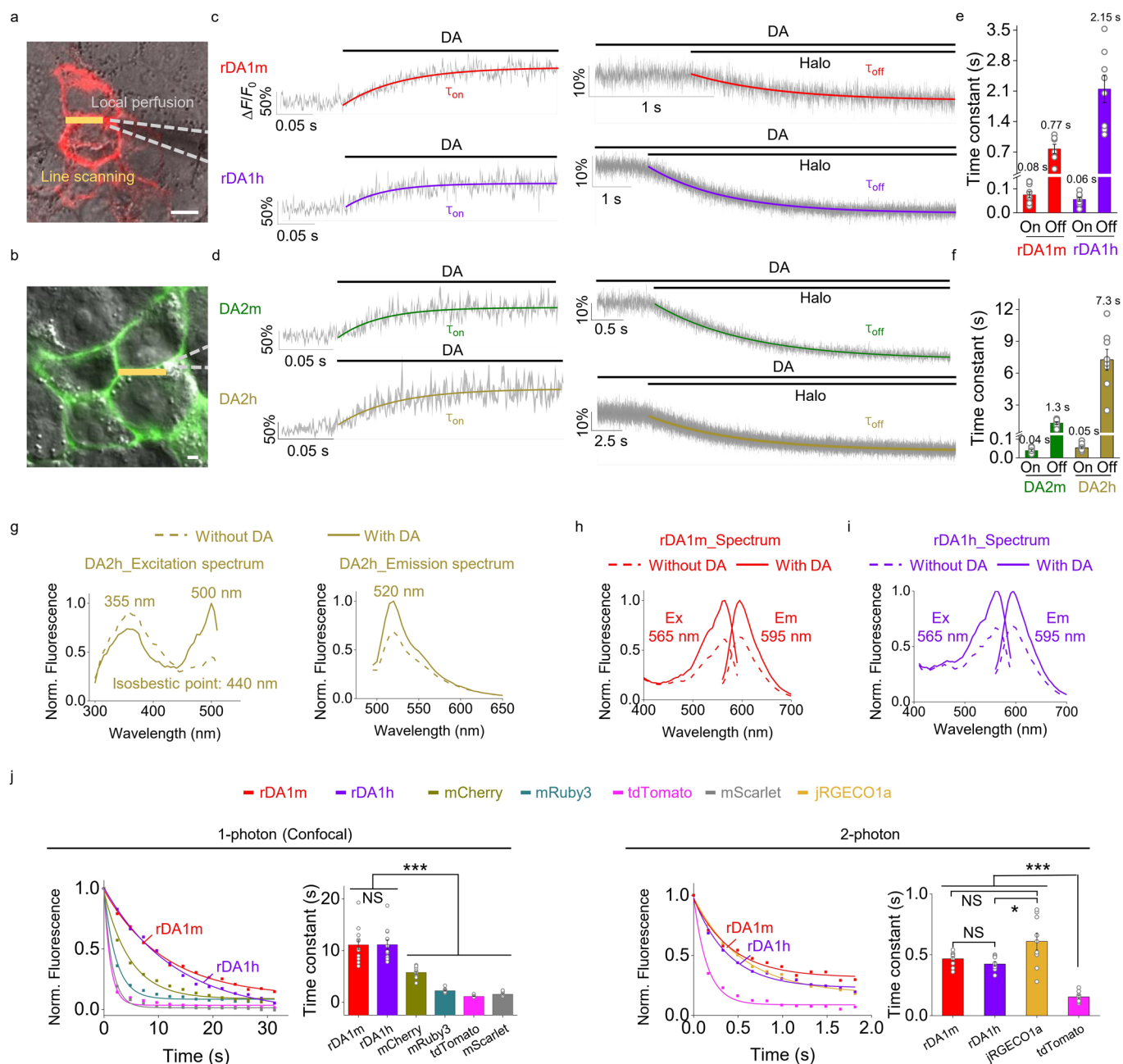


**Extended Data Fig. 1 | The development of red fluorescent DA sensors and second-generation green fluorescent DA sensors.** **a**, Schematic illustration showing the design and optimization of the red fluorescent GRAB<sub>DA</sub> sensors. **b**, The response to 100  $\mu$ M DA measured for red fluorescent DA sensor variants during steps 1–3. The variant with the highest fluorescence change (named rDA0.5) was then sequentially mutated as shown to generate rDA1m, rDA1h, and rDA-mut. **c**, Schematic illustration showing the design and optimization of the green fluorescent GRAB<sub>DA</sub> sensors. **d**, Normalized  $\Delta F/F_0$  in response to 100  $\mu$ M DA measured for green fluorescent DA sensor variants, normalized to the first-generation DA1h sensor. DA2h was then mutated as shown to generate DA2m and DA-mut. The superscripts in the insets of **b**, **d** are based on the Ballesteros-Weinstein numbering scheme<sup>54</sup>, indicating the mutation sites in the D<sub>2</sub>R.

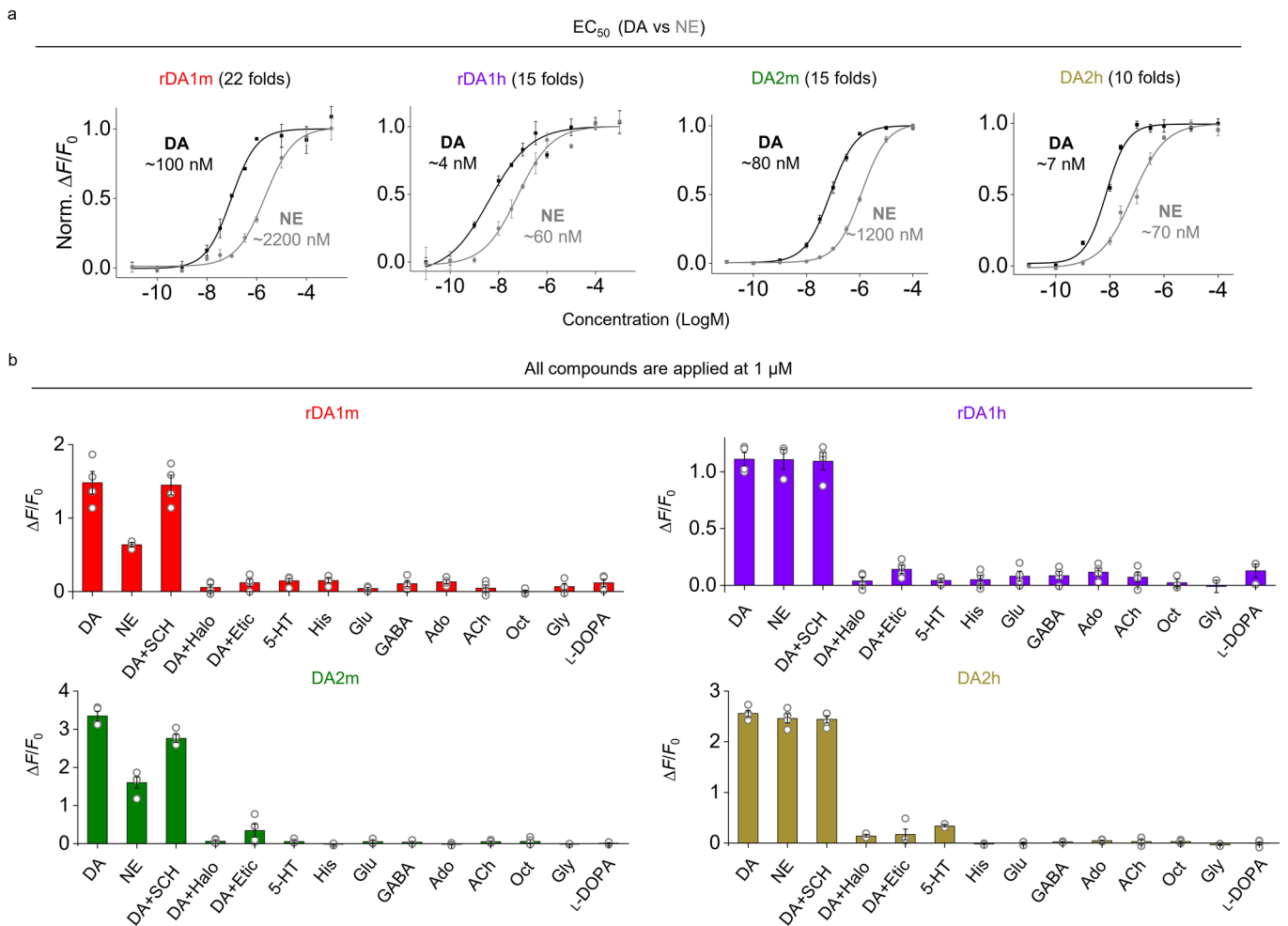


**Extended Data Fig. 2 | The sequences of GRAB<sub>DA</sub> sensors and the residues related to affinity-tuning, cpRFP and cpEGFP optimization. a,b,** The sequences of rGRAB<sub>DA1m</sub> (**a**) and GRAB<sub>DA2m</sub> (**b**). The residues related to affinity-tuning, cpRFP (**a**) and cpEGFP (**b**) optimization are marked.

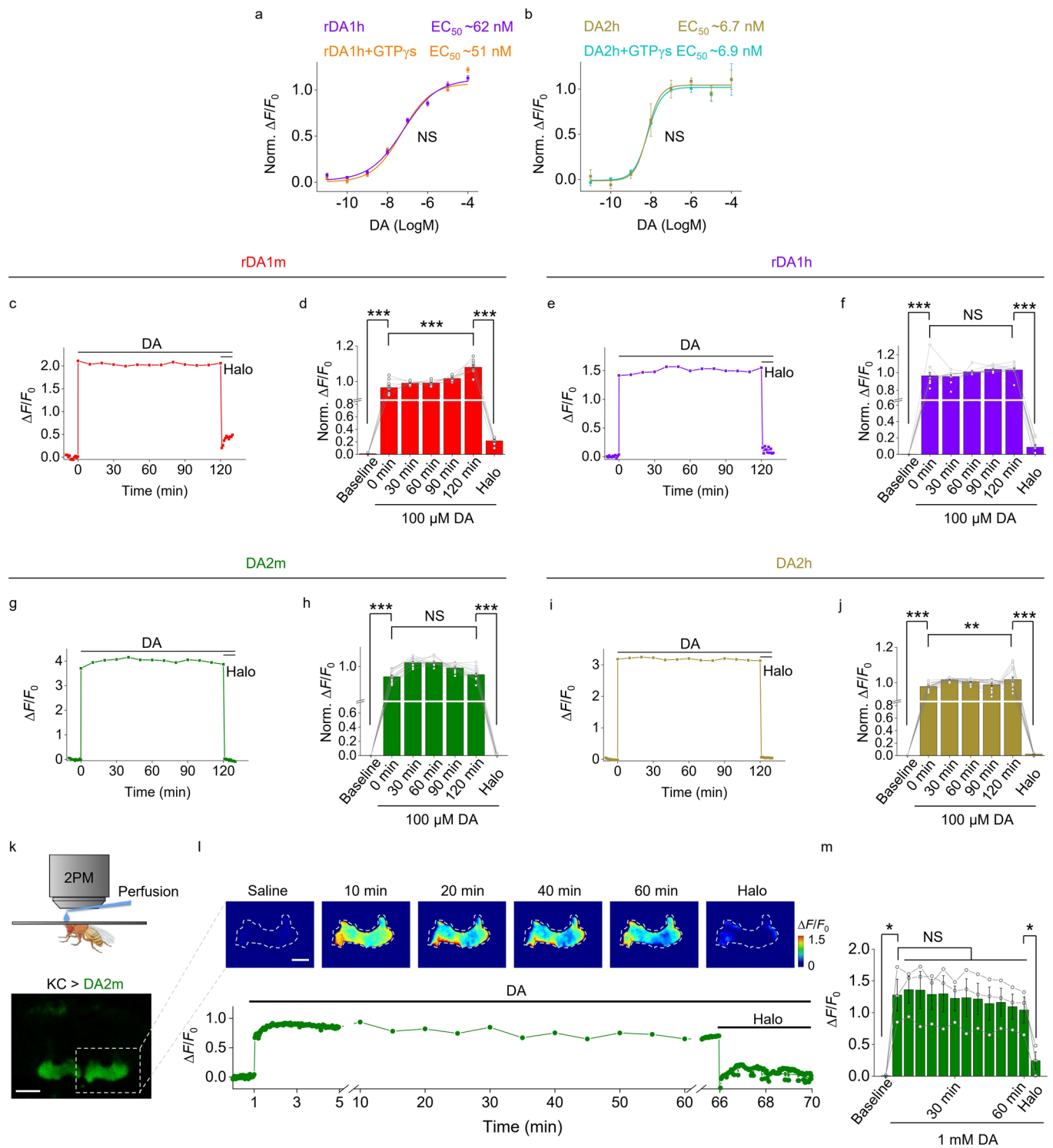




**Extended Data Fig. 3 | Characterization of the sensors in HEK293T cells. a, b**, Schematic illustration showing the local perfusion system. Scale bars, 10  $\mu\text{m}$ . **c, d**, Representative traces showing the response to DA (left) and subsequent addition of Halo (right). The traces were the average of 3 different regions of interest (ROIs) on the scanning line, shaded with  $\pm$  s.e.m.. Each trace was fitted with a single-exponential function to determine  $\tau_{\text{on}}$  (left) and  $\tau_{\text{off}}$  (right). Similar results were observed for 7-10 cells. **e, f**, Group summary of  $\tau_{\text{on}}$  and  $\tau_{\text{off}}$ . **g-i**, Excitation and emission spectra for the indicated sensors in the absence and presence of DA. **j**, Photostability of rDA1m and rDA1h (in the presence of 100  $\mu\text{M}$  DA) and the indicated fluorescent proteins was measured using 1-photon and 2-photon microscopy. Each photobleaching curve was fitted with a single-exponential function to determine the time constant. 1-photon,  $n=12$  cells each. 2-photon,  $n=10, 10, 9, 10$  cells for rDA1m, rDA1h, jRGECO1a, tdTomato. Two-tailed Student's  $t$ -test was performed. 1-photon,  $P=0.9755$  between rDA1m and rDA1h;  $P=2.72 \times 10^{-5}$  between rDA1m and mCherry;  $P=7.10 \times 10^{-9}$  between rDA1m and mRuby3;  $P=7.90 \times 10^{-10}$  between rDA1m and tdTomato;  $P=1.95 \times 10^{-9}$  between rDA1m and mScarlet;  $P=1.28 \times 10^{-5}$  between rDA1h and mCherry;  $P=2.50 \times 10^{-9}$  between rDA1h and mRuby3;  $P=2.66 \times 10^{-10}$  between rDA1h and tdTomato;  $P=6.75 \times 10^{-10}$  between rDA1h and mScarlet. 2-photon,  $P=0.0963$  between rDA1m and rDA1h;  $P=0.0511$  between rDA1m and jRGECO1a;  $P=0.0139$  between rDA1h and jRGECO1a;  $P=2.82 \times 10^{-11}$  between rDA1m and tdTomato;  $P=1.71 \times 10^{-10}$  between rDA1h and tdTomato;  $P=2.96 \times 10^{-6}$  between jRGECO1a and tdTomato. Data are presented as the mean  $\pm$  s.e.m. in **e, f, j** (bar graph). \* $P < 0.05$ ; \*\*\* $P < 0.001$ .



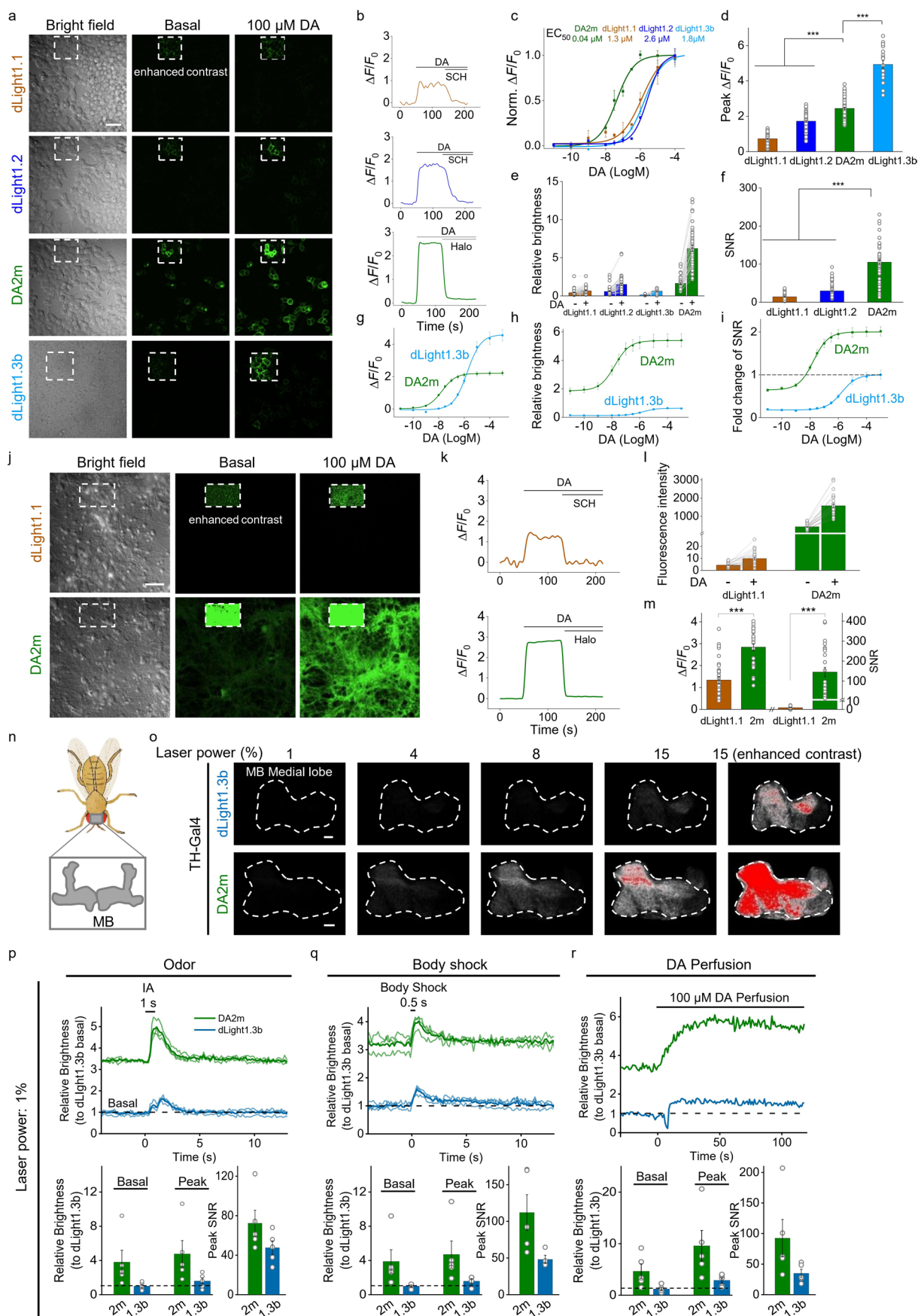
**Extended Data Fig. 4 | The response of GRAB<sub>DA</sub> sensors to different compounds.** **a**, The normalized dose-response curves for DA and NE in sensor-expressing HEK293T cells.  $n=3$  wells with 200–800 cells/well. **b**, The  $\Delta F/F_0$  in sensor-expressing cells in response to the indicated compounds applied at 1  $\mu$ M.  $n=3$  wells for rDA1h in response to NE, 5-HT, Oct, Gly and L-DOPA.  $n=4$  wells for the others. Each well contains 200–1200 cells. Data are presented as the mean  $\pm$  s.e.m.. Data replotted from Fig. 2a.



Extended Data Fig. 5 | See next page for caption.

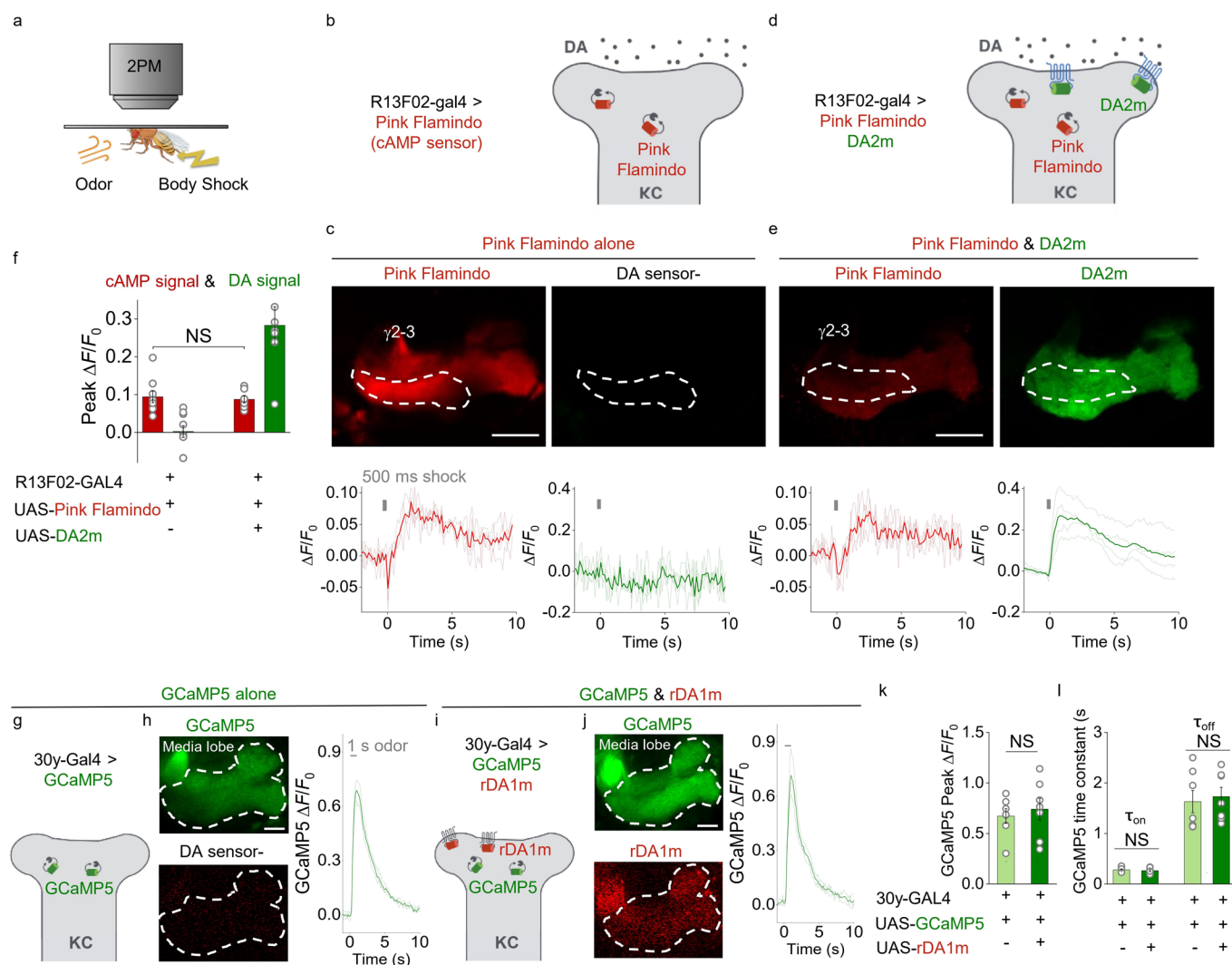
**Extended Data Fig. 5 | The minimal coupling of GRAB<sub>DA</sub> sensors to downstream G<sub>i</sub> pathway and  $\beta$ -arrestin pathway. **a,b**, Normalized  $\Delta F/F_0$  in sensor-expressing cells in response to DA, with or without the pre-bathing of GTP $\gamma$ S.  $n=3$  wells with 500–3000 cells/well. **c,d**, The representative trace of  $\Delta F/F_0$  (**c**) and the group summary of normalized  $\Delta F/F_0$  (**d**) in rDA1m-expressing neurons during a 2-hour treatment of 100  $\mu$ M DA.  $n=9$  neurons. For the group summary, the averaged  $\Delta F/F_0$  of each neuron during the 2-hour DA treatment is normalized to 1. Two-tailed Student's  $t$ -test was performed.  $P=2.10 \times 10^{-21}$  between baseline and 0 min;  $P=2.99 \times 10^{-17}$  between 120 min and Halo;  $P=1.24 \times 10^{-5}$  between 0 min and 120 min. **e,f**, Similar to **c** and **d** except that rDA1h was expressed in cultured neurons.  $n=11$  neurons. Two-tailed Student's  $t$ -test was performed.  $P=1.87 \times 10^{-6}$  between baseline and 0 min;  $P=3.43 \times 10^{-17}$  between 120 min and Halo;  $P=0.1519$  between 0 min and 120 min. **g,h**, Similar to **c** and **d** except that DA2m was expressed in cultured neurons.  $n=15$  neurons. Two-tailed Student's  $t$ -test was performed.  $P=2.48 \times 10^{-39}$  between baseline and 0 min;  $P=7.42 \times 10^{-35}$  between 120 min and Halo;  $P=0.3322$  between 0 min and 120 min. **i,j**, Similar to **c** and **d** except that DA2h was expressed in cultured neurons.  $n=17$  neurons. Two-tailed Student's  $t$ -test was performed.  $P=1.14 \times 10^{-52}$  between baseline and 0 min;  $P=9.80 \times 10^{-38}$  between 120 min and Halo;  $P=0.0061$  between 0 min and 120 min. **k**, Top, schematic illustration depicting the in vivo perfusion experiment. Bottom, the fluorescence image of a transgenic fly expressing DA2m in MB KCs. Scale bar, 50  $\mu$ m. **l,m**, Representative images (**l**, top), trace (**l**, bottom) and group summary (**m**) of  $\Delta F/F_0$  in response to the 1-hour perfusion of 1 mM DA followed by 100  $\mu$ M Halo in a transgenic fly expressing DA2m in MB KCs.  $n=3$  flies. Scale bar, 25  $\mu$ m. Two-tailed Student's  $t$ -test was performed.  $P=0.0382$  between baseline and 10 min;  $P=0.0293$  between 60 min and Halo;  $P=0.5289, 0.5593, 0.9559, 0.8537, 0.6346, 0.6530, 0.2760, 0.1649, 0.1547, 0.1152, 0.1044$  between 5 min and 10 min, 15 min, 20 min, 25 min, 30 min, 35 min, 40 min, 45 min, 50 min, 55 min, 60 min, respectively. Data are presented as the mean  $\pm$  s.e.m.. in **a,b,d,f,h,j,m**. \* $P < 0.05$ ; \*\* $P < 0.01$ ; \*\*\* $P < 0.001$ .**





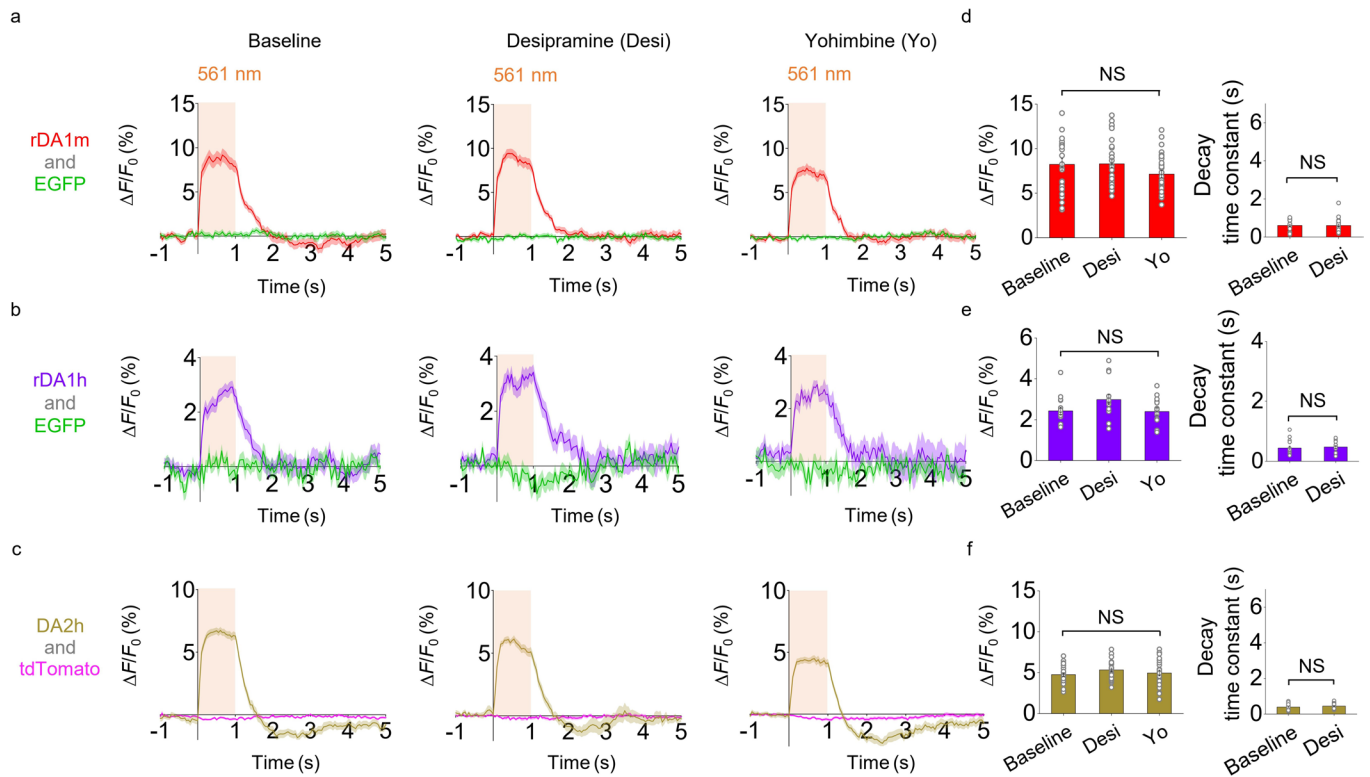
Extended Data Fig. 6 | See next page for caption.

**Extended Data Fig. 6 | Comparison between dLight and GRAB<sub>DA</sub>.** **a**, Representative bright-field and fluorescence images acquired before (baseline) and after application of DA in sensor-expressing HEK293T cells. Similar results were observed for more than 20 cells. Scale bar, 50  $\mu\text{m}$ . **b**, Representative traces of  $\Delta F/F_0$  in response to 100  $\mu\text{M}$  DA followed by either 10  $\mu\text{M}$  SCH or 10  $\mu\text{M}$  Halo. Similar results were observed for more than 30 cells. **c**, Normalized dose-response curves.  $n = 3$  wells with 100–500 cells/well. **d–f**, Group summary of the peak  $\Delta F/F_0$  (**d**), relative brightness (green/red ratio, GR ratio) (**e**), and signal-to-noise ratio (SNR) (**f**) in response to 100  $\mu\text{M}$  DA. **d**,  $n = 73, 62, 61, 20$  cells for dLight1.1, dLight1.2, DA2m, dLight1.3b. **e**,  $n = 77, 66, 20, 60$  cells for dLight1.1, dLight1.2, dLight1.3b, DA2m. **f**,  $n = 74, 63, 61$  cells for dLight1.1, dLight1.2, DA2m. Two-tailed Student's  $t$ -test was performed. **d**,  $P = 2.10 \times 10^{-48}$  between dLight1.1 and DA2m;  $P = 1.31 \times 10^{-12}$  between dLight1.2 and DA2m;  $P = 1.22 \times 10^{-10}$  between dLight1.3 and DA2m. **f**,  $P = 4.09 \times 10^{-22}$  between dLight1.1 and DA2m;  $P = 1.13 \times 10^{-33}$  between dLight1.2 and DA2m. **g–i**, Dose-response curves (**g**), relative brightness (**h**), and fold change of SNR (**i**) for dLight1.3b and DA2m.  $n = 20$  cells each. **j–m**, Similar to **a–f**, except that dLight1.1 and DA2m were expressed in cultured neurons. **m**, left,  $n = 30, 28$  cells for dLight1.1, DA2m. **m**, right,  $n = 30$  cells each. Scale bar, 50  $\mu\text{m}$ . Two-tailed Student's  $t$ -test was performed. **m**, left,  $P = 4.43 \times 10^{-8}$ ; right,  $P = 3.59 \times 10^{-8}$ . **n**, Schematic illustration depicting the location of the *Drosophila* olfactory mushroom body (MB). **o**, Fluorescence images of the MB using 2-photon microscopy at the indicated laser power settings. Enhanced-contrast images at 15% laser power are shown. Fluorescence is shown in grayscale, with saturated pixels shown in red. Similar results were observed for 4–5 flies. Scale bars, 10  $\mu\text{m}$ . **p–r**, Representative traces (top) and group summary of relative brightness during odorant application (**p**), body shock (**q**), and DA perfusion (**r**). **p, r**,  $n = 5$  flies each. **q**,  $n = 5, 4$  flies for DA2m, dLight1.3b. Average traces (bold) overlaid with single-trial traces (light) from one fly are shown for representation in **p, q**. Data are presented as the mean  $\pm$  s.e.m. in **c, d, e, f, g, h, i, l, m, p, q, r**. \*\*\* $P < 0.001$ .



### Extended Data Fig. 7 | Expressing GRAB<sub>DA2m</sub> or GRAB<sub>rDA1m</sub> sensors shows no significant effect on cAMP or calcium signaling respectively *in vivo*.

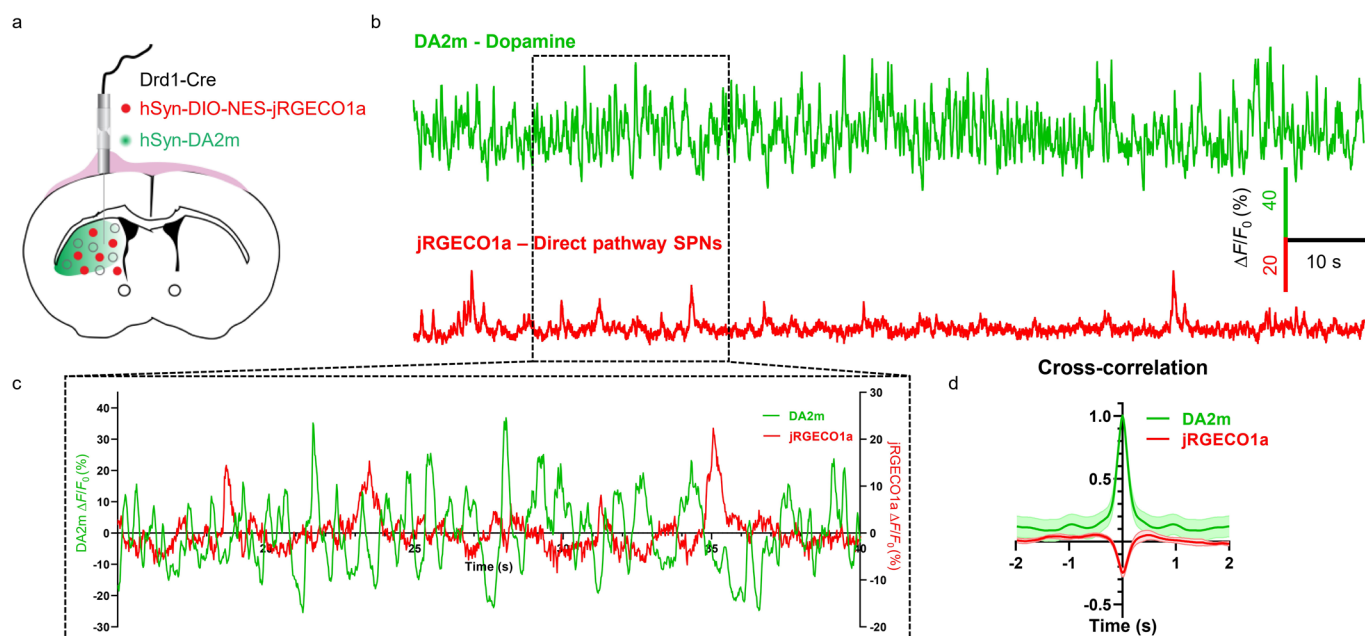
**a**, Schematic illustration depicting the experimental setup. **b–e**, Schematic illustrations depicting the experimental strategy (**b,d**), representative fluorescence images and  $\Delta F/F_0$  traces (**c,e**) in flies expressing the cAMP sensor Pink-Flamindo (**b,c**) or co-expressing Pink-Flamindo and DA2m (**d,e**) in MB KCs. The ROIs for measuring the  $\gamma 2-3$  compartments in the MB are indicated by dashed white lines. Scale bars, 25  $\mu\text{m}$ . **f**, Group summary of peak  $\Delta F/F_0$ .  $n=9$ , 7 flies for Pink Flamindo alone, Pink Flamindo & DA2m. Two-tailed Student's *t*-test was performed.  $P=0.7332$ . **g–j**, Schematic illustrations depicting the experimental strategy (**g,i**), representative fluorescence images and  $\Delta F/F_0$  traces (**h,j**) in flies expressing the calcium sensor GCaMP5 (**g,h**) or co-expressing GCaMP5 and rDA1m (**i,j**) in MB KCs. The ROIs for measuring the MB media lobe are indicated by dashed white lines. Similar results were observed for 7 flies. Scale bars, 25  $\mu\text{m}$ . **k,l**, Group summary of GCaMP5 peak  $\Delta F/F_0$  and time constants.  $n=7$  flies each. Two-tailed Student's *t*-test was performed. **k**,  $P=0.607$ . **l**,  $P=0.601$ , 0.735 for  $\tau_{on}$ ,  $\tau_{off}$ . Average traces (bold) overlaid with single-trial traces (light) from one fly are shown for representation in **c,e,h,j**. Data are presented as the mean  $\pm$  s.e.m. in **f,k,l**.



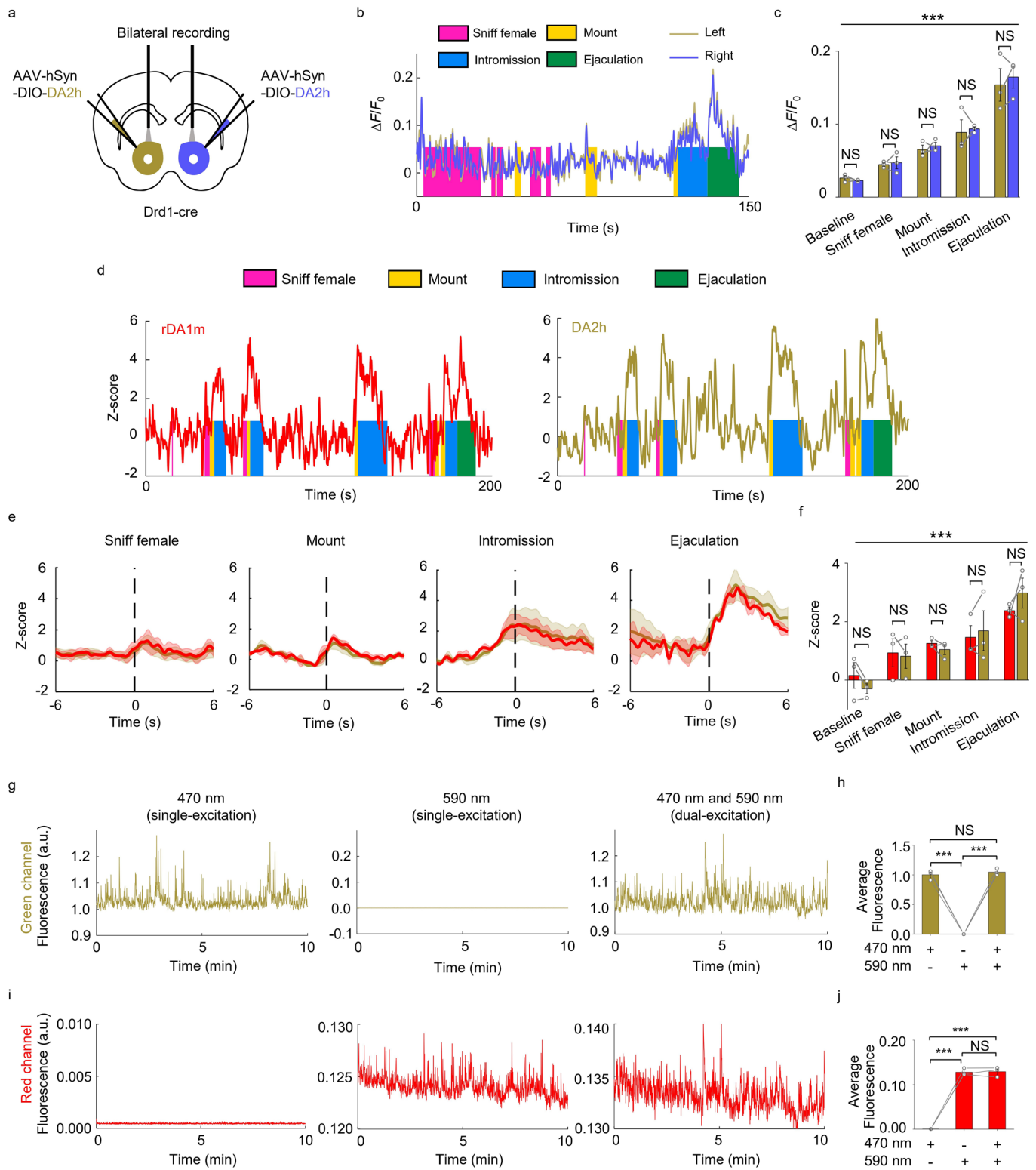
**Extended Data Fig. 8 | Optogenetically induced nigrostriatal DA release in freely moving mice is not affected by desipramine or yohimbine.**

**a–c**, Average traces of  $\Delta F/F_0$  in mice expressing rDA1m and EGFP (**a**), rDA1h and EGFP (**b**), or DA2h and tdTomato (**c**) in the dorsal striatum. Where indicated, the experiments were conducted in mice treated with either the norepinephrine transporter blocker desipramine or the  $\alpha_2$ -adrenergic receptor antagonist yohimbine. **d–f**, Group summary of  $\Delta F/F_0$  and  $\tau_{\text{off}}$  for the experiments shown in **a–c**, respectively.  $n=30$  trials from 6 hemispheres of 6 mice for rDA1m.  $n=15$  trials from 3 hemispheres of 3 mice for rDA1h,  $n=25$  trials from 5 hemispheres of 4 mice for DA2h. Two-tailed Student's *t*-test was performed. **d**, left,  $P=0.1614$ ; right,  $P=0.9836$ . **e**, left,  $P=0.9018$ ; right,  $P=0.6605$ . **f**, left,  $P=0.6489$ ; right,  $P=0.2322$ . Average traces shaded with  $\pm$  s.e.m. are shown in **a–c**. Data are presented as the mean  $\pm$  s.e.m. in **d–f**.





**Extended Data Fig. 9 | Dual-color recording of DA dynamics and striatal neural activity using DA2m and jRGECO1a in freely moving mice.** **a**, Schematic illustration depicting the experimental strategy. **b**, Representative traces showing the fluorescence responses of DA2m and jRGECO1a. **c**, The zoom-in traces from **b** during a 25 s recording. **d**, The cross-correlation between the fluorescence responses of DA2m and jRGECO1a during a 2 min recording.  $n=8$  hemispheres of 5 mice. Average traces shaded with  $\pm$  s.e.m. are shown.



Extended Data Fig. 10 | See next page for caption.

**Extended Data Fig. 10 | The DA signal in the mouse NAc during sexual behavior.** **a**, Schematic illustration depicting the experimental strategy. **b, c**, Representative traces (**b**) and group summary (**c**) of  $\Delta F/F_0$  measured from left and right hemispheres during the indicated stages of mating.  $n=3$  mice.  $F_{4,16}=80.92$ ,  $P < 10^{-6}$  for row factor and  $F_{1,4}=0.1224$ ,  $P=0.7441$  for column factor by two-way ANOVA. Bonferroni's multiple comparisons test was performed between groups,  $P > 0.9999$ ,  $P > 0.9999$ ,  $P > 0.9999$ ,  $P > 0.9999$ ,  $P > 0.9999$ . **d**, Representative traces of the concurrent Z-score signals of rDA1m and DA2h during the indicated stages of sexual behavior. Similar results were observed for 3 mice. **e**, Average post-stimulus histograms showing the Z-score signals of rDA1m and DA2h aligned to the onset of the indicated mating events.  $n=3$  mice. Average traces shaded with  $\pm$  s.e.m. are shown. **f**, Group summary of the Z-scores measured for rDA1m and DA2h during the indicated mating events.  $n=3$  mice.  $F_{4,16}=13.02$ ,  $P=6.6 \times 10^{-5}$  for row factor and  $F_{1,4}=0.001$ ,  $P=0.9797$  for column factor by two-way ANOVA. Bonferroni's multiple comparisons test was performed,  $P > 0.99$ ,  $P > 0.99$ ,  $P > 0.99$ ,  $P > 0.99$ ,  $P > 0.99$ . **g,h**, The representative fluorescence signal (**g**) and group analysis (**h**) in the green channel when the excitation light is delivered at 470 nm alone (**g**, left), at 590 nm alone (**g**, center) or at 470 nm and 590 nm simultaneously (**g**, right).  $n=3$  mice.  $F_{2,4}=531.6$ ,  $P=3.1 \times 10^{-5}$  by one-way ANOVA. Tukey's multiple comparisons test was performed between groups,  $P=3.1 \times 10^{-5}$ ,  $P=2.6 \times 10^{-5}$ ,  $P=0.4904$ . **i,j**, Similar to **g** and **h** except the fluorescence signal in the red channel is analyzed.  $n=3$  mice.  $F_{2,4}=414.2$ ,  $P=2.3 \times 10^{-5}$  by one-way ANOVA. Tukey's multiple comparisons test was performed between groups,  $P=4.8 \times 10^{-5}$ ,  $P=4.6 \times 10^{-5}$ ,  $P=0.9738$ . Data are presented as the mean  $\pm$  s.e.m. in **c,f,h,j**. \*\*\* $P < 0.001$ .

## Reporting Summary

Nature Research wishes to improve the reproducibility of the work that we publish. This form provides structure for consistency and transparency in reporting. For further information on Nature Research policies, see [Authors & Referees](#) and the [Editorial Policy Checklist](#).

### Statistics

For all statistical analyses, confirm that the following items are present in the figure legend, table legend, main text, or Methods section.

n/a Confirmed

- The exact sample size ( $n$ ) for each experimental group/condition, given as a discrete number and unit of measurement
- A statement on whether measurements were taken from distinct samples or whether the same sample was measured repeatedly
- The statistical test(s) used AND whether they are one- or two-sided  
*Only common tests should be described solely by name; describe more complex techniques in the Methods section.*
- A description of all covariates tested
- A description of any assumptions or corrections, such as tests of normality and adjustment for multiple comparisons
- A full description of the statistical parameters including central tendency (e.g. means) or other basic estimates (e.g. regression coefficient) AND variation (e.g. standard deviation) or associated estimates of uncertainty (e.g. confidence intervals)
- For null hypothesis testing, the test statistic (e.g.  $F$ ,  $t$ ,  $r$ ) with confidence intervals, effect sizes, degrees of freedom and  $P$  value noted  
*Give  $P$  values as exact values whenever suitable.*
- For Bayesian analysis, information on the choice of priors and Markov chain Monte Carlo settings
- For hierarchical and complex designs, identification of the appropriate level for tests and full reporting of outcomes
- Estimates of effect sizes (e.g. Cohen's  $d$ , Pearson's  $r$ ), indicating how they were calculated

*Our web collection on [statistics for biologists](#) contains articles on many of the points above.*

### Software and code

Policy information about [availability of computer code](#)

Data collection

1. The commercial software of Ti-E A1 confocal microscope (Nikon).
2. The commercial software of FV1000MPE 2-photon microscope (Olympus).
3. The commercial software of Opera Phenix high-content screening system (PerkinElmer).
4. The commercial video acquisition software StreamPix5 (NorPix).
5. The commercial software of VS120 virtual slide microscope (Olympus).
6. The commercial software of OceanView (Ocean Insight).
7. Custom MATLAB codes and TDT programs. <https://github.com/pdollar/toolbox>, [https://github.com/bd125/GRAB\\_DA\\_Fig6\\_Code](https://github.com/bd125/GRAB_DA_Fig6_Code).

Data analysis

1. ImageJ 1.52p (NIH).
2. MATLAB R2019a (MathWorks). <https://github.com/pdollar/toolbox>. [https://github.com/bd125/GRAB\\_DA\\_Fig6\\_Code](https://github.com/bd125/GRAB_DA_Fig6_Code).
3. OriginPro 9.1 (OriginLab).
4. GraphPad Prism 7 and 8 (GraphPad).
5. A linear unmixing algorithm. <https://www.niehs.nih.gov/research/atniehs/labs/ln/pi/iv/tools/index.cfm>.
6. NeuroExplorer 5 (Nex Technologies).

For manuscripts utilizing custom algorithms or software that are central to the research but not yet described in published literature, software must be made available to editors/reviewers. We strongly encourage code deposition in a community repository (e.g. GitHub). See the Nature Research [guidelines for submitting code & software](#) for further information.



## Data

Policy information about [availability of data](#)

All manuscripts must include a [data availability statement](#). This statement should provide the following information, where applicable:

- Accession codes, unique identifiers, or web links for publicly available datasets
- A list of figures that have associated raw data
- A description of any restrictions on data availability

Plasmids expressing the sensors used in this study were deposited at Addgene ([https://www.addgene.org/Yulong\\_Li/](https://www.addgene.org/Yulong_Li/)). Source data are provided with this paper.

## Field-specific reporting

Please select the one below that is the best fit for your research. If you are not sure, read the appropriate sections before making your selection.

Life sciences  Behavioural & social sciences  Ecological, evolutionary & environmental sciences

For a reference copy of the document with all sections, see [nature.com/documents/nr-reporting-summary-flat.pdf](https://nature.com/documents/nr-reporting-summary-flat.pdf)

## Life sciences study design

All studies must disclose on these points even when the disclosure is negative.

Sample size	No statistical methods were used to predetermine sample size. We used sample sizes similar to the literatures in the field. [1] Inoue, M., Takeuchi, A., Manita, S., Horigane, S.I., Sakamoto, M., Kawakami, R., Yamaguchi, K., Otomo, K., Yokoyama, H., Kim, R., et al. (2019). Rational Engineering of XCaMPs, a Multicolor GECI Suite for In Vivo Imaging of Complex Brain Circuit Dynamics. <i>Cell</i> 177, 1346-1360 e1324. [2] Mohr, M.A., Bushey, D., Aggarwal, A., Marvin, J.S., Kim, J.J., Marquez, E.J., Liang, Y., Patel, R., Macklin, J.J., Lee, C.Y., et al. (2020). jYCaMP: an optimized calcium indicator for two-photon imaging at fiber laser wavelengths. <i>Nat Methods</i> . [3] Feng, J., Zhang, C., Lischinsky, J.E., Jing, M., Zhou, J., Wang, H., Zhang, Y., Dong, A., Wu, Z., Wu, H., et al. (2019). A Genetically Encoded Fluorescent Sensor for Rapid and Specific In Vivo Detection of Norepinephrine. <i>Neuron</i> 102, 745-761 e748. [4] Patriarchi, T., Cho, J.R., Merten, K., Howe, M.W., Marley, A., Xiong, W.H., Folk, R.W., Broussard, G.J., Liang, R.Q., Jang, M.J., et al. (2018). Ultrafast neuronal imaging of dopamine dynamics with designed genetically encoded sensors. <i>Science</i> 360, 1420-+. [5] Sun, F., Zeng, J., Jing, M., Zhou, J., Feng, J., Owen, S.F., Luo, Y., Li, F., Wang, H., Yamaguchi, T., et al. (2018). A Genetically Encoded Fluorescent Sensor Enables Rapid and Specific Detection of Dopamine in Flies, Fish, and Mice. <i>Cell</i> 174, 481-496 e419.
Data exclusions	No data were excluded from the analysis.
Replication	All attempts at replication were successful. The experiments were performed using >3 independent cell cultures and >2 independent cohorts of animals.
Randomization	Cells and animals were randomly allocated into experimental groups.
Blinding	The investigators were not blinded to group allocation during data collection and analysis. The experimental conditions were obvious to the researchers and the analyses were performed objectively and not subjective to human bias.

## Behavioural & social sciences study design

All studies must disclose on these points even when the disclosure is negative.

Study description	<i>Briefly describe the study type including whether data are quantitative, qualitative, or mixed-methods (e.g. qualitative cross-sectional, quantitative experimental, mixed-methods case study).</i>
Research sample	<i>State the research sample (e.g. Harvard university undergraduates, villagers in rural India) and provide relevant demographic information (e.g. age, sex) and indicate whether the sample is representative. Provide a rationale for the study sample chosen. For studies involving existing datasets, please describe the dataset and source.</i>
Sampling strategy	<i>Describe the sampling procedure (e.g. random, snowball, stratified, convenience). Describe the statistical methods that were used to predetermine sample size OR if no sample-size calculation was performed, describe how sample sizes were chosen and provide a rationale for why these sample sizes are sufficient. For qualitative data, please indicate whether data saturation was considered, and what criteria were used to decide that no further sampling was needed.</i>
Data collection	<i>Provide details about the data collection procedure, including the instruments or devices used to record the data (e.g. pen and paper, computer, eye tracker, video or audio equipment) whether anyone was present besides the participant(s) and the researcher, and whether the researcher was blind to experimental condition and/or the study hypothesis during data collection.</i>
Timing	<i>Indicate the start and stop dates of data collection. If there is a gap between collection periods, state the dates for each sample cohort.</i>

Data exclusions	<i>If no data were excluded from the analyses, state so OR if data were excluded, provide the exact number of exclusions and the rationale behind them, indicating whether exclusion criteria were pre-established.</i>
Non-participation	<i>State how many participants dropped out/declined participation and the reason(s) given OR provide response rate OR state that no participants dropped out/declined participation.</i>
Randomization	<i>If participants were not allocated into experimental groups, state so OR describe how participants were allocated to groups, and if allocation was not random, describe how covariates were controlled.</i>

## Ecological, evolutionary & environmental sciences study design

All studies must disclose on these points even when the disclosure is negative.

Study description	<i>Briefly describe the study. For quantitative data include treatment factors and interactions, design structure (e.g. factorial, nested, hierarchical), nature and number of experimental units and replicates.</i>
Research sample	<i>Describe the research sample (e.g. a group of tagged <i>Passer domesticus</i>, all <i>Stenocereus thurberi</i> within Organ Pipe Cactus National Monument), and provide a rationale for the sample choice. When relevant, describe the organism taxa, source, sex, age range and any manipulations. State what population the sample is meant to represent when applicable. For studies involving existing datasets, describe the data and its source.</i>
Sampling strategy	<i>Note the sampling procedure. Describe the statistical methods that were used to predetermine sample size OR if no sample-size calculation was performed, describe how sample sizes were chosen and provide a rationale for why these sample sizes are sufficient.</i>
Data collection	<i>Describe the data collection procedure, including who recorded the data and how.</i>
Timing and spatial scale	<i>Indicate the start and stop dates of data collection, noting the frequency and periodicity of sampling and providing a rationale for these choices. If there is a gap between collection periods, state the dates for each sample cohort. Specify the spatial scale from which the data are taken</i>
Data exclusions	<i>If no data were excluded from the analyses, state so OR if data were excluded, describe the exclusions and the rationale behind them, indicating whether exclusion criteria were pre-established.</i>
Reproducibility	<i>Describe the measures taken to verify the reproducibility of experimental findings. For each experiment, note whether any attempts to repeat the experiment failed OR state that all attempts to repeat the experiment were successful.</i>
Randomization	<i>Describe how samples/organisms/participants were allocated into groups. If allocation was not random, describe how covariates were controlled. If this is not relevant to your study, explain why.</i>
Blinding	<i>Describe the extent of blinding used during data acquisition and analysis. If blinding was not possible, describe why OR explain why blinding was not relevant to your study.</i>
Did the study involve field work?	<input type="checkbox"/> Yes <input type="checkbox"/> No

## Field work, collection and transport

Field conditions	<i>Describe the study conditions for field work, providing relevant parameters (e.g. temperature, rainfall).</i>
Location	<i>State the location of the sampling or experiment, providing relevant parameters (e.g. latitude and longitude, elevation, water depth).</i>
Access and import/export	<i>Describe the efforts you have made to access habitats and to collect and import/export your samples in a responsible manner and in compliance with local, national and international laws, noting any permits that were obtained (give the name of the issuing authority, the date of issue, and any identifying information).</i>
Disturbance	<i>Describe any disturbance caused by the study and how it was minimized.</i>

## Reporting for specific materials, systems and methods

We require information from authors about some types of materials, experimental systems and methods used in many studies. Here, indicate whether each material, system or method listed is relevant to your study. If you are not sure if a list item applies to your research, read the appropriate section before selecting a response.

## Materials &amp; experimental systems

## Methods

- n/a  Involved in the study
- Antibodies
- Eukaryotic cell lines
- Palaeontology
- Animals and other organisms
- Human research participants
- Clinical data

- n/a  Involved in the study
- ChIP-seq
- Flow cytometry
- MRI-based neuroimaging

## Antibodies

## Antibodies used

## Primary antibody:

- (1) Rabbit anti-RFP antibody (1:1000) (Takara Bio USA, CA) (cat#: 632496).  
 (2) Chicken anti-GFP antibody (1:1000) (Abcam, MA) (cat#: ab13970).

## Secondary antibody:

- (1) Cy3-conjugated donkey anti-rabbit IgG (1:1000) (Jackson ImmunoResearch, PA) (cat#: 113713).  
 (2) Alexa 488-conjugated donkey anti-chicken IgY (1:1000) (Jackson ImmunoResearch, PA) (cat#: 116967).

## Validation

All antibodies were validated either by the manufacturer or used extensively in published research articles.

Rabbit anti-RFP antibody (Takara Bio USA, CA) (PMID: 31245789) (The manufacturer website states that this antibody has been validated with DsRed-expressing HEK293 cells by Western blot)  
 Chicken anti-GFP antibody (Abcam, MA) (PMID: 30674877) (The manufacturer website states that this antibody has been validated with GFP-transfected NIH/3T3 cells by Immunocytochemistry)

Cy3-conjugated donkey anti-rabbit IgG (Jackson ImmunoResearch, PA) (PMID: 32003745)  
 Alexa 488-conjugated donkey anti-chicken IgY (Jackson ImmunoResearch, PA) (PMID: 31995756)

## Eukaryotic cell lines

Policy information about [cell lines](#)

## Cell line source(s)

- The HEK293T cell line was bought from ATCC (cat. number CRL-3216).
- The reporter cell line used to measure GPCR activation via a modified Tango  $\beta$ -arrestin recruitment assay was a gift from Bryan Roth. Addgene, Roth Lab PRESTO-Tango GPCR Kit (Kit #100000068). The original publication is "PRESTO-Tango as an open-source resource for interrogation of the druggable human GPCrome. Kroeze WK, Sassano MF, Huang XP, Lansu K, McCorvy JD, Giguère PM, Sciaky N, Roth BL. Nat Struct Mol Biol. 2015 May;22(5):362-9. doi: 10.1038/nsmb.3014. Epub 2015 Apr 20."

## Authentication

The cell lines were authenticated based on the morphology under microscope and the analysis of the growth curve.

## Mycoplasma contamination

The cell lines were not tested for mycoplasma contamination.

Commonly misidentified lines  
(See [ICLAC](#) register)

This study did not involve commonly misidentified lines.

## Palaeontology

## Specimen provenance

*Provide provenance information for specimens and describe permits that were obtained for the work (including the name of the issuing authority, the date of issue, and any identifying information).*

## Specimen deposition

*Indicate where the specimens have been deposited to permit free access by other researchers.*

## Dating methods

*If new dates are provided, describe how they were obtained (e.g. collection, storage, sample pretreatment and measurement), where they were obtained (i.e. lab name), the calibration program and the protocol for quality assurance OR state that no new dates are provided.*

Tick this box to confirm that the raw and calibrated dates are available in the paper or in Supplementary Information.

## Animals and other organisms

Policy information about [studies involving animals](#); [ARRIVE guidelines](#) recommended for reporting animal research

## Laboratory animals

- Postnatal 0-day-old (P0) Sprague-Dawley rats (Beijing Vital River Laboratory), male and female.
- Adult (P42–90) wild-type C57BL/6N (Beijing Vital River Laboratory), male and female.
- Adult (P42–90) wild-type C57BL/6N (Charles River Laboratories), male and female.

4. Adult (P42–90) DAT-IRES-Cre mice (Jackson Laboratory, stock number 06660), male and female.
5. Adult (P42–90) Drd1-cre mice (MMRRC\_036916-UCD), male and female.
6. Adult (P42–90) Drd1-cre mice (MMRRC\_030989-UCD), male and female.
7. Adult female transgenic Drosophila lines within 2 weeks after eclosion were used for fluorescence imaging.

Wild animals

This study did not involve wild animals.

Field-collected samples

This study did not involve samples collected from the fields.

Ethics oversight

All procedures for animal surgery, maintenance, and behavior were performed using protocols that were approved by the respective animal care and use committees at Peking University, New York University, and the US National Institutes of Health.

Note that full information on the approval of the study protocol must also be provided in the manuscript.

## Human research participants

Policy information about [studies involving human research participants](#)

Population characteristics

Describe the covariate-relevant population characteristics of the human research participants (e.g. age, gender, genotypic information, past and current diagnosis and treatment categories). If you filled out the behavioural & social sciences study design questions and have nothing to add here, write "See above."

Recruitment

Describe how participants were recruited. Outline any potential self-selection bias or other biases that may be present and how these are likely to impact results.

Ethics oversight

Identify the organization(s) that approved the study protocol.

Note that full information on the approval of the study protocol must also be provided in the manuscript.

## Clinical data

Policy information about [clinical studies](#)

All manuscripts should comply with the ICMJE [guidelines for publication of clinical research](#) and a completed [CONSORT checklist](#) must be included with all submissions.

Clinical trial registration

Provide the trial registration number from [ClinicalTrials.gov](#) or an equivalent agency.

Study protocol

Note where the full trial protocol can be accessed OR if not available, explain why.

Data collection

Describe the settings and locales of data collection, noting the time periods of recruitment and data collection.

Outcomes

Describe how you pre-defined primary and secondary outcome measures and how you assessed these measures.

## ChIP-seq

### Data deposition

Confirm that both raw and final processed data have been deposited in a public database such as [GEO](#).

Confirm that you have deposited or provided access to graph files (e.g. BED files) for the called peaks.

Data access links

May remain private before publication.

For "Initial submission" or "Revised version" documents, provide reviewer access links. For your "Final submission" document, provide a link to the deposited data.

Files in database submission

Provide a list of all files available in the database submission.

Genome browser session

(e.g. [UCSC](#))

Provide a link to an anonymized genome browser session for "Initial submission" and "Revised version" documents only, to enable peer review. Write "no longer applicable" for "Final submission" documents.

### Methodology

Replicates

Describe the experimental replicates, specifying number, type and replicate agreement.

Sequencing depth

Describe the sequencing depth for each experiment, providing the total number of reads, uniquely mapped reads, length of reads and whether they were paired- or single-end.

Antibodies

Describe the antibodies used for the ChIP-seq experiments; as applicable, provide supplier name, catalog number, clone name, and lot number.

Peak calling parameters

Specify the command line program and parameters used for read mapping and peak calling, including the ChIP, control and index files used.



Data quality

*Describe the methods used to ensure data quality in full detail, including how many peaks are at FDR 5% and above 5-fold enrichment.*

Software

*Describe the software used to collect and analyze the ChIP-seq data. For custom code that has been deposited into a community repository, provide accession details.*

## Flow Cytometry

### Plots

Confirm that:

- The axis labels state the marker and fluorochrome used (e.g. CD4-FITC).
- The axis scales are clearly visible. Include numbers along axes only for bottom left plot of group (a 'group' is an analysis of identical markers).
- All plots are contour plots with outliers or pseudocolor plots.
- A numerical value for number of cells or percentage (with statistics) is provided.

### Methodology

Sample preparation

*Describe the sample preparation, detailing the biological source of the cells and any tissue processing steps used.*

Instrument

*Identify the instrument used for data collection, specifying make and model number.*

Software

*Describe the software used to collect and analyze the flow cytometry data. For custom code that has been deposited into a community repository, provide accession details.*

Cell population abundance

*Describe the abundance of the relevant cell populations within post-sort fractions, providing details on the purity of the samples and how it was determined.*

Gating strategy

*Describe the gating strategy used for all relevant experiments, specifying the preliminary FSC/SSC gates of the starting cell population, indicating where boundaries between "positive" and "negative" staining cell populations are defined.*

- Tick this box to confirm that a figure exemplifying the gating strategy is provided in the Supplementary Information.

## Magnetic resonance imaging

### Experimental design

Design type

*Indicate task or resting state; event-related or block design.*

Design specifications

*Specify the number of blocks, trials or experimental units per session and/or subject, and specify the length of each trial or block (if trials are blocked) and interval between trials.*

Behavioral performance measures

*State number and/or type of variables recorded (e.g. correct button press, response time) and what statistics were used to establish that the subjects were performing the task as expected (e.g. mean, range, and/or standard deviation across subjects).*

### Acquisition

Imaging type(s)

*Specify: functional, structural, diffusion, perfusion.*

Field strength

*Specify in Tesla*

Sequence &amp; imaging parameters

*Specify the pulse sequence type (gradient echo, spin echo, etc.), imaging type (EPI, spiral, etc.), field of view, matrix size, slice thickness, orientation and TE/TR/flip angle.*

Area of acquisition

*State whether a whole brain scan was used OR define the area of acquisition, describing how the region was determined.*

Diffusion MRI

 Used Not used

### Preprocessing

Preprocessing software

*Provide detail on software version and revision number and on specific parameters (model/functions, brain extraction, segmentation, smoothing kernel size, etc.).*

Normalization

*If data were normalized/standardized, describe the approach(es): specify linear or non-linear and define image types used for transformation OR indicate that data were not normalized and explain rationale for lack of normalization.*

Normalization template	<i>Describe the template used for normalization/transformation, specifying subject space or group standardized space (e.g. original Talairach, MNI305, ICBM152) OR indicate that the data were not normalized.</i>
Noise and artifact removal	<i>Describe your procedure(s) for artifact and structured noise removal, specifying motion parameters, tissue signals and physiological signals (heart rate, respiration).</i>
Volume censoring	<i>Define your software and/or method and criteria for volume censoring, and state the extent of such censoring.</i>

## Statistical modeling & inference

Model type and settings	<i>Specify type (mass univariate, multivariate, RSA, predictive, etc.) and describe essential details of the model at the first and second levels (e.g. fixed, random or mixed effects; drift or auto-correlation).</i>
Effect(s) tested	<i>Define precise effect in terms of the task or stimulus conditions instead of psychological concepts and indicate whether ANOVA or factorial designs were used.</i>
Specify type of analysis:	<input type="checkbox"/> Whole brain <input type="checkbox"/> ROI-based <input type="checkbox"/> Both
Statistic type for inference (See <a href="#">Eklund et al. 2016</a> )	<i>Specify voxel-wise or cluster-wise and report all relevant parameters for cluster-wise methods.</i>
Correction	<i>Describe the type of correction and how it is obtained for multiple comparisons (e.g. FWE, FDR, permutation or Monte Carlo).</i>

## Models & analysis

- n/a | Involved in the study
- Functional and/or effective connectivity
- Graph analysis
- Multivariate modeling or predictive analysis

Functional and/or effective connectivity	<i>Report the measures of dependence used and the model details (e.g. Pearson correlation, partial correlation, mutual information).</i>
Graph analysis	<i>Report the dependent variable and connectivity measure, specifying weighted graph or binarized graph, subject- or group-level, and the global and/or node summaries used (e.g. clustering coefficient, efficiency, etc.).</i>
Multivariate modeling and predictive analysis	<i>Specify independent variables, features extraction and dimension reduction, model, training and evaluation metrics.</i>